NTNU – Trondheim
Norwegian University of
Science and Technology

Optical and Electrical studies of GaAs Nanowire arrays on Si substrates

Eivind Halmøy Wolden

Master of Science in Electronics
Submission date: June 2015
Supervisor: Helge Weman, IET
Co-supervisor: Johannes Reinertsen, IET

Norwegian University of Science and Technology
Department of Electronics and Telecommunications

Photoluminescence spectroscopy of position controlled GaAs nanowires on Silicon substrates

Eivind Halmøy Wolden

June 16, 2015

Abstract

Six different patterned samples and one unpatterend sample of GaAs/AlGaAs, core/shell, nanowires (NWs) grown by the self-catalysed technique was investigated using scanning electron microscopy and photoluminescence (PL) spectroscopy. The aim was to optimize growth in a way that yielded emission at the free exciton energy of 1.515 eV. To investigate this the samples have been subjected to a temperature of 12 K. The physical sizes have been analyzed and compared. The PL measurements have been used to find the integrated intensity per second for each sample along with the emission energy. Using this with the growth conditions some conclusions have been attempted.

The aim of the optimization have not been achieved. None of the patterned samples showed a consistent free exciton emission.

Sammendrag

Syv ulike prøver bestående av GaAs/AlGaAs grodd ved den selvkatalyserte teknikken har blitt analysert ved bruk av elektron mikroskopi og fotoluminsense spectroskopi. Målet var å optimalisere veksten ved å finne en fri exciton emissjon. Prøvene har blitt analysert ved en temperature på 12 K. Fysiske størrelser og fotoluminisens spekter har blitt brukt for å gjøre denne analysen. Noen kolkusjoner har blitt forsøkt dratt ut i fra disse målingene.

Målet med optimaliseringen har ikke blitt nådd. Ingen av prøvene har vist noen konsistent fri exciton emission

Acknowledgements

This project assignment has been performed at the Norwegian University of Science and Technology (NTNU), with the department of Electronics and Telecommunications (IET). The work has been done as part of Prof. Bjørn Ove Fimland and Prof. Helge Weman's group, a research group working with the growth and characterization of GaAs nanowires for optoelectronic applications.

I would like to thank Prof. Helge Weman for providing me with the opportunity to perform this work and participate in the highly specialized and recognized research they are performing.

For providing SEM images, new samples and data on the growth of the nanowires analyzed, I would like to thank PhD candidate Dingding Ren. His help has made me understand what factors influence the growth of nanowires. Additionally, the SEM images provided was needed to do analysis of the growths. Any questions about the SEM images or growths was skillfully answered.

Lastly, I would like to thank my supervisor PhD candidate Johannes F. Reinertsen for helping me understand concepts, perform measurements, and analyze measurements. He have showed patience, provided me with explanations, and pointed me in the right direction when my understanding did not suffice. Without His help, and motivation, this work would not have been possible.

Contents

1 Introduction

Semiconductors are found in every aspect of the modern day life. The most common material used in semiconductors to this date is silicon (Si). While Si has a great range of properties making it popular, it also has limitations. For many optical applications, the indirect band gap means that Si is unsuitable and alternative materials have to be used.

A material that was early determined to have favorable optical properties is gallium arsenide (GaAs) [1]. GaAs is a III-V semiconductor with a direct band gap, and a high electron mobility [2]. This means applications requiring a very high frequency and power, are areas where GaAs perform well. Both lasers [3, 4] and solar cells [5] made with GaAs have been proven to be effective.

Since 1990 the research on nanowires (NWs) [6] have increased. With over 3000 papers published each year since 2010 there is a great deal of research focusing on NWs for a variety of uses; lasers [7], transistors [8], and solar cells [9] to name a few. For optoelectronic purposes GaAs NWs show particular suitability [10].

One major reason why NWs is so desirable is because of the high aspect ratio. By having a surface with NWs, it is possible to increase the surface area significantly compared to a smooth surface. Many applications such as sensors benefit from having a larger surface area, while optical devices can benefit from the quantum confinement effects found in NWs [11]. Furthermore, materials on the nano scale behave differently than how they would in a bulk material. In a nanowire it is possible to tune material properties in new ways [12]. It should be clear then, that using nanowires could prove beneficial for various purposes.

The growth of GaAs NWs on a Si wafer is not problem free, the lattice mismatch means that the interface will be under strain [13]. However, due to NWs ability to accommodate strain, growth is possible as long as the area of the interface is not too large [14].

Nanowires described in this paper are grown using the vapor-liquid-solid (VLS) method in a bottom up approach. This is a well documented method dating back to 1964 [15]. Using a metal as a catalyst, often gold (Au), this method has been proven to be effective at growing GaAs nanowires [16–18].

However, using Au as a catalyst have several drawbacks that can prove detrimental to desired optical effect [19, 20]. By using a self catalysed (SC) technique, where Ga forms a droplet that is used as a catalyst, the negative effects of incorporating Au are avoided. This was proven to be possible in 2008 [21]. The grown GaAs NWs come in different crystal structures, namely zincblende (ZB) and wurtzite (WZ). In recent years, using molecular beam epitaxy (MBE), control over which structure is grown has been increased [22, 23] and instead of structuring in nanometers such as in MOCVD the structuring can be done in monolayers (ML) [24]. Since MBE-grown Au assisted NWs mainly grow in the WZ structure, it is interesting to have the option to grow ZB GaAs NWs. Furthermore, bulk GaAs exist mainly in the ZB form. Nanowires behave differently than a bulk material, however, it is possible to use the known properties of bulk ZB GaAs in studies of ZB GaAs NW since the crystal structure is then the same.

To capitalize on the optical properties found in GaAs NWs, a shell is grown around each NW. The shell is made of aluminum gallium arsenide (AlGaAs). By using AlGaAs it is possible to adapt, through growth control to have a near lattice match with GaAs [25]. This is good since it will not put too much strain on the NWs. Furthermore AlGaAs has a

larger band gap than GaAs. A larger band gap means that electrons and holes will be confined in the core and non-radiative surface recombination will be greatly reduced [26, 27].

Photoluminescence (PL) spectroscopy is a method to gain knowledge about the optical properties of nanowires. This can be especially useful when the NWs will be used as optical devices, however, PL spectroscopy can also be used to gain information on the structual composition of the NWs.

Before and during growth of patterned nanowires there is a wide variety of parameters that can be changed and optimization can be focused in various direction depending on the purpose of the growth. Previous studies done at NTNU have examined the growth of GaAs nanowires [28] and PL spectra from single GaAs core-shell nanowires [29]. During the growth of the nanowires presented in theses studies a good (PL) spectra was measured. In this context a good PL spectra means that the nanowires behave as predicted by theory and are not noisy. One of the samples examined by both these papers is used here for reference and included in the results.

Necessary theory is presented in chapter two. Chapter three presents information on the growth process, the PL setup and analysis of data. In chapter four the results are presented, these are discussed in chapter five and explanations for observed behaviors are sought. Chapter six gives a conclusion for the findings. References and additional data can be found at the end.

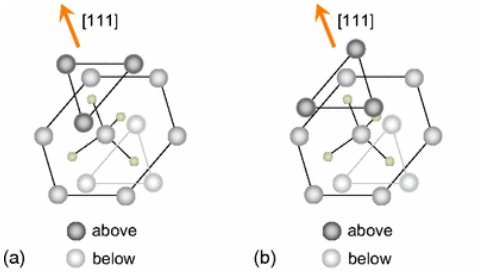

Figure 1: (a) Zincblende and (b) Wurtzite unit cells along [111] direction illustrating the stacking difference [31].

2 Theory

2.1 Crystal structures

Crystal structures are highly ordered structures in a material. A crystalline liquid or solid is an arrangement of atoms, ions or molecules. This type of arrangement can affect the properties of a material. To talk more in depth about crystal structures it is necessary to define some terms.

A unit cell is the most basic and least volume consuming repeating structure of any solid. In crystalline patterns, the unit cell makes it easy to visualize the difference between crystal structures. In a pure structure the unit cell is enough to describe the solid, this is because a repetition of the unit cell gives the entire structure. To fully describe a unit cell the atoms or molecules are assigned a lattice parameter. The convention is to use a range from 0 to 1, where 1 means that the atom is shared with the next unit cell. There are two configurations for the GaAs unit cell, namely Zincblende (ZB) and Wurtzite (WZ). It is important to be aware of this difference in crystal structure since it explains why the observed properties in gallium arsenide can be different under the same conditions.

By using lattice parameters in the x, y and z direction, the difference between ZB and WZ GaAs can be written down. For ZB GaAs there is one arsenic atom at (0,0,0) and one gallium atom at $(\frac{1}{4},\frac{1}{4},\frac{1}{4})$. This is all that is needed to completely describe the ZB GaAs structure. For WZ GaAs the atom placements are different, there are arsenic atoms at (0,0,0) and $(\frac{2}{3},\frac{1}{3},\frac{1}{2})$, and gallium atoms at $(0,0,\frac{5}{6})$ and $(\frac{2}{3},\frac{1}{3},\frac{1}{8})$.

A further way to visualize the difference between these two crystal structures is to look at them from a different angle. Along the [111] direction the difference is easy to see. In figure 1 both structures are illustrated. In addition to describing the unit cell of a structure it can be informative to look at the stacking along different directions. In the figure, only the top layer is different. The layers are conventionally labeled by letters, this means that for Zincblende there is a ABA stacking. The top layer and the bottom layer is the same, which means only two layers are repeated to get the full structure. Wurtzite has a ABC stacking, where there are three different layers that can be repeated to get the full structure. The top layer of WZ has been rotated by $\frac{\pi}{3}$ with respect to the bottom layer. This small difference means that the two structures of GaAs have different properties.

For structures intended to be pure ZB or WZ, there is a chance that stacking faults (SF)

occur. Stacking faults happen because the intended structure gets temporarily interchanged by another structure. This interchange can be for one or several layers and often has detrimental effects on a device.

2.2 Growth orientation

2.3 Defects and doping

In addition to stacking faults, any deviation from an infinite, perfect crystal structure is called a defect [32]. There are very few materials with a perfect structure, it is therefore clear that crystalline materials may contain several types of defects. There are four main classifications of defects depending on their dimensionality. The first group is called point defects (0D), these occur when there is some defect on or around a single lattice point. Line defects (1D) are caused by a misalignment of two or more atoms in a row. In planar defects (2D) a plane in the crystal does not follow the expected structure. Stacking faults are planar defects. The edges of the crystal structure are also planar defects. The last group of defects is called bulk defects (3D). In a bulk defect, considerable portions of the crystal structure have a different structure. These can be voids, i.e. lack of atoms or impurities.

Doping a semiconductor is done by intentionally introducing impurity defects to the crystal structure [33]. The purpose of doping is to change the electrical properties of the material. The impurities are point defects, which stems from adding atoms to the structure that either have only one electron in the outer shell or are missing only one electron in the outer shell. These added atoms will either donate (n-doping) or accept (p-doping) an electron. This means that the total electrical charge of the doped crystal structure will go up for n-doping and down for p-doping.

2.4 Growth of nanowires

The conditions during the growth of nanowires dictates the purity and material properties observed later. The NWs used in the experiments detailed in this paper was grown with the vapor-liquid-solid (VLS) method [15] using a bottom-up approach. This was done with a molecular beam epitaxy (MBE) method. Silicon (Si) was used as a substrate because it is well documented [34] and does not interfere with the GaAs/AlGaAs nanowires.

The most common method for growing NWs is using a metal as a catalyst, however this has several disadvantages [19, 20]. An alternative is to use a self catalysed (SC) process. In the self catalysed process for GaAs, gallium atoms forms a droplet. This droplet is where the growth of the NW starts. As more material is supplied through the flow of gallium the droplet gets supersaturated and starts to precipitate at the liquid-solid interface. The nanowire will then grow under the droplet [35]. The size of the droplet determines the diameter of the nanowire, which can be controlled for patterned samples.

Using the SC technique it is also possible to control the crystal structure for GaAs to yield a majority of either ZB or WZ NWs [36]. Furthermore, it is possible to grow only in two dimensions (2D) [27]. By changing conditions in the growth chamber, the droplet can be consumed, which means that any further growth will be radial. Growth can therefore be either axial or radial, which is utilized to create NW devices. For photoluminescence,

a common utilization of this is to grow a capping on the nanowire, this capping will be a shell that has roughly equal thickness both on top of, and on the sides of the NW.

2.5 Patterned vs random growth

The substrate used for growth can impact the nanowires. More specifically the patterning of the surface will determine the density and structure of the nanowires. On a non-patterned surface the nanowires will grow where the gallium can nucleate. In a patterned sample, there is a layer of oxide on top of the silicon which has holes etched into it. Through optimization of growth conditions, a nanowire can grow in a hole and only there. It is important to distinguish between one nanowire and various. It is desired that only one NW grows in the hole, this leads to higher uniformity among the NWs. Concerning the surface and optimization there are a few factors that can be changed. The type and thickness of the oxide can be changed, the hole diameter and geometry can be varied, and lastly the pitch can be varied. Through the optimization of these, along with growth parameters the NWs can be made uniform. However, uniform can be interpreted in various ways. There is uniformity in morphological, electrical, and optical properties. These properties may or may not coincide with each other. Nanowires that look very different in the SEM may respond nearly identically when subjected to light and vise versa.

2.5.1 Electron-beam lithography

In *electron-beam litography* (EBL) the surface of the substrate is covered with a electron-sensitive film called a resist. When the electron beam hits it changes solubility of the resist where it hits. By immersing the substrate into a solvent, the resist can be removed at selected areas because it was either exposed or not to the electron beam. This enables the drawing of patterns at a very small scale [37]. EBL is a slow process compared to NIL, since exposure is done with a beam of electrons, to create a pattern from this it is necessary to scan back and forth across the surface.

2.5.2 Nano-imprint lithography

nano-imprint lithography (NIL) patterning is attractive because of its low cost, high throughput and high resolution. There are various ways to do nanoimpriting, however, what they have in common is that a stamp of some form is used. This stamp is normally pressed onto a resist which changes solubility either due to exposure to light or applied heat [38]. Because a stamp is used, it is easy to achieve a large throughput. Which means that the patterning is not restricted to a small area of the wafer as in EBL, but can cover most of the wafer.

2.6 Molecular beam epitaxy

MBE is a technique widely used for growing epitaxial structures such as insulators, semiconductors, and metals [39]. This technique requires ultra-high vacuum conditions, with a base pressure of about 10^{-10} Torr. Extremely pure materials are sublimated from effusion cells and are supplied as a beam of atoms or molecules. Because of the high vacuum,

there is very little interaction with ambient contaminants or between beams. By adjusting temperature, the rate of growth can be adjusted. Because of the possibility of a low growth rate, a few Å/s, monolayers are possible to control [40]. Shutters allow for turning on and off the flux, which in turn allows for abrupt interfaces in a multilayer structure. Furthermore, due to the high vacuum, the epitaxial growth process can be monitored using in-situ characterization techniques such as reflection high-energy electron diffraction (RHEED) [41].

2.7 Band theory

The electrons of a single atom occupies atomic orbitals, which form a discrete set of energy levels. Prior to bringing atoms together their atomic orbitals may overlap. However, when brought together, there will because of Pauli's exclusion principle not be overlapping energy levels [32]. The resulting energy levels is called the molecular orbitals [42]. Energies from different atoms are not allowed to be the same. Since nature always seeks the lowest possible energy, there will be several closely spaced energy levels. As more molecules are brought together the energy levels for the molecules will become increasingly dense. When enough molecules are together, they form a solid and the energy levels will be dense enough to form a continuum of energy levels. These continuums are called *energy bands* [43].

The energy bands have a finite width, this width depends on the degree of overlap in the atomic orbitals. If two adjacent bands are not wide enough to cover the range of energy between them, we are left with regions where there are no bands, called *band gaps* [44]. Although there is an infinite number of energy levels and therefore also an infinite number of energy bands, there is a finite number of electrons available. This means that there will be unoccupied bands. The electrons will first occupy the bands with the lowest possible energy, which means that there is less chance of finding an occupied band for increasing energy. The band with the highest energy that is fully occupied and the band with the lowest energy that is unoccupied at 0 K have special names. Namely the *valence band* (VB) and *conduction band* (CB), respectively. The band gap generally refers to the gap between these two bands [32]. Another important quantity when talking about band gaps is the *Fermi level*. The Fermi level can be thought of as a quasi energy level, that has a 50% probability of being occupied at any given time. It does not necessarily refer to an actual energy level in a material, but it is a precisely defined thermodynamic quantity [32].

Based on a material's band gap, it is classified as one of four material types. These four are insulators, semiconductors, semi-metals, and metals. The materials are classified at 0 K. In figure 2 the band gaps and material types are illustrated. If the conduction band, defined as the range of energy required to free an electron from its bond to an atom, is partially or completely filled with electrons the material is a metal. Electrons in the CB can absorb and lose energy by jumping to a higher energy level and going back down again. This means they can transport energy, which is the principle behind electrical conductivity. A semi-metal is a material where the conduction- and valence band, defined as the highest range of electron energy where electrons are present at 0 K, partially overlap.

In figure 2 the different states of doping is also shown for the semiconductor, showing how the charge carrier concentration gets shifted depending on the doping. The difference between a semiconductor and an insulator is the width of the band gap. Generally speaking

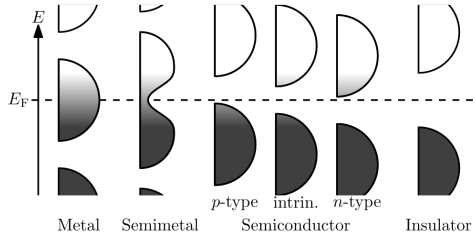

Figure 2: Filling of the density of states at 0 K in the four differently conducting materials. The horizontal axis represents DOS for each individual material. The vertical axis describes energy. Shading represents electron occupation. E_F is the Fermi level. [45]

a semiconductor has a band gap in the vicinity of 1 eV while an insulator has a band gap of about 9 eV or above. The reasoning behind these values is that at 9 eV, the thermal energy at room temperature is not sufficient to allow electrons from the VB to be promoted to the CB [46].

2.7.1 Density of states

The *density of states* (DOS) describes the number of available states for each interval of energy [47]. With the exception of quantum wells, the DOS in GaAs nanowires is continuous [48]. In figure 2, the shape of an idealized DOS is shown for each material. There is less available states towards the edges of the band. Electrons will always occupy the lowest energy state possible through effects such as thermalization as is explained in section 2.8. States will therefore be occupied starting at the band edge and however far into the band the excitation rate permits [49].

2.7.2 GaAs Band structure

The band gap of a semiconductor is a complicated construction of potentials. It is often portrayed as a planar level, the planar section in such illustrations is in reality a tiny section at the center of the shortest band gap [50]. The true electronic structure has been calculated using various means. In figure 3 this structure is shown for zincblende and in figure 4 for wurtzite. These figures show the true layout of the bands. The x-axis is the wave vector $\vec{k}$, representing movement in momentum space and the y-axis is the energy. An electron can move along the x-axis by interaction with phonons [51], whereas interaction with photons can move the electron along the y-axis. This explains why a direct band gap is better for optoelectronic applications. The photon can do all the work and no interaction with phonons is necessary to excite an electron to the CB edge. Since the Γ gap is the smallest, this is where the electrons and holes will pile up. However, there is a smaller number of states available at the center of the gap as explained in section 2.7.1.

2.7.3 GaAs/AlGaAs band structure

Without a shell, GaAs NWs are prone to non-radiative surface recombination when exposed to light [55]. This means that some percentage of the electrons are recombin-

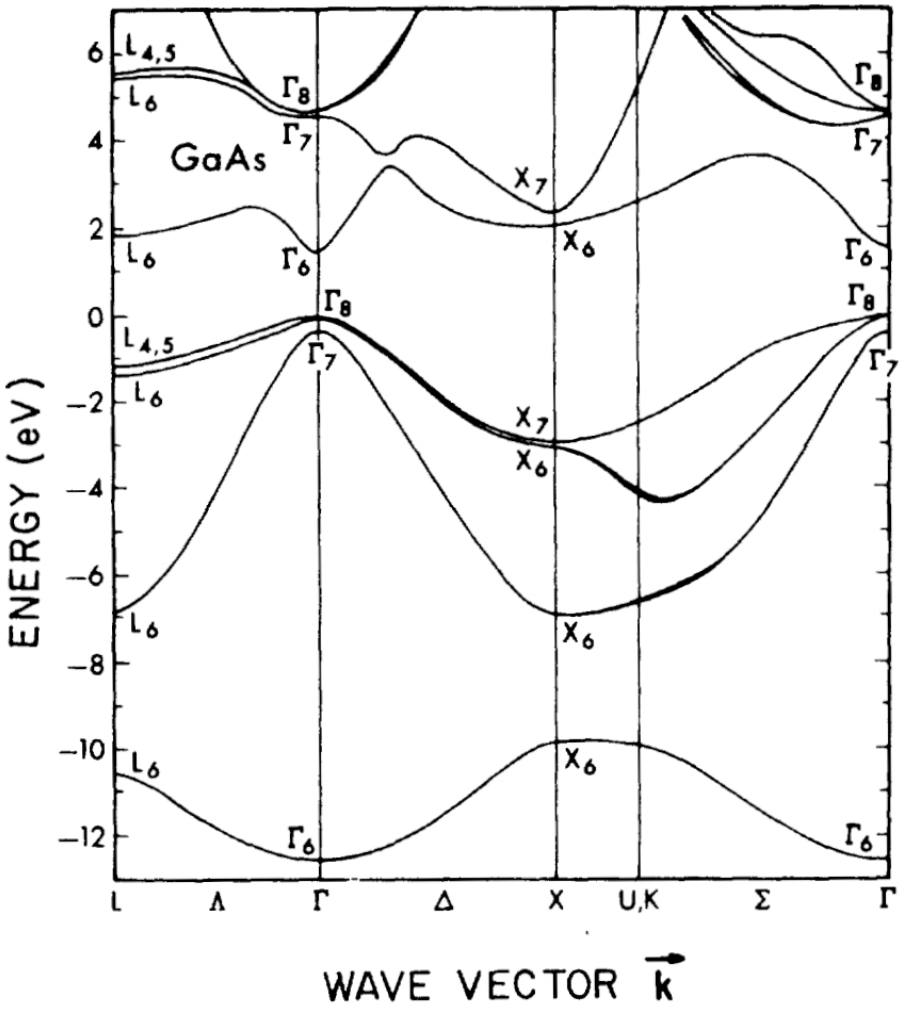

Figure 3: Calculated band structure for GaAs zincblende[52–54]. Γ is the direct gap, measured between Γ_6 and Γ_8. This is the gap observed when measuring optoelectronic devices.

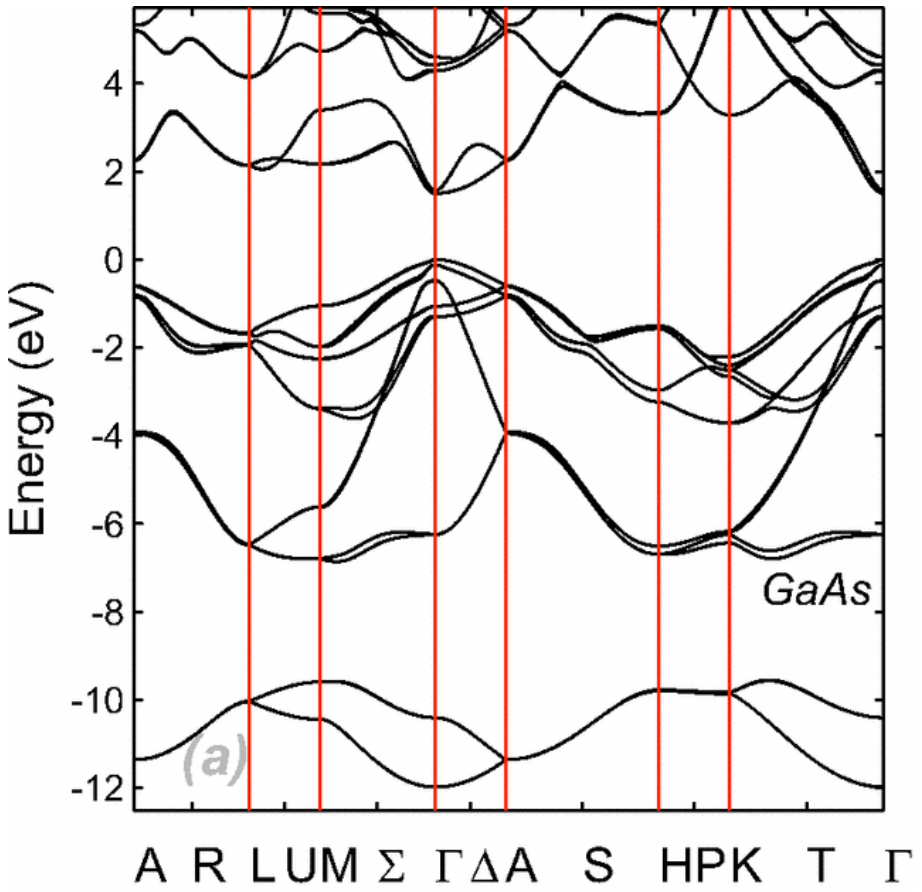

Figure 4: Calculated band structure for GaAs wurtzite[31]. The direct band gap is located at Γ.

ing without emitting a photon [56]. This is the reason that around the GaAs core, an $Al_xGa_{1-x}As$ shell is grown where x represents the percentage of aluminum in the composition. When this shell is grown at 900°C there is a perfect lattice match with GaAs for all values of x because GaAs and AlAs have identical lattice parameters at this temperature [50]. This means that strain will not be a problem when shell growth is done close to this temperature. AlAs has an indirect band gap of 2.16 eV in a bulk material at 300 K [57], while GaAs has a band gap of 1.424 in a bulk material at 300 K [58]. This leaves the band gap of AlGaAs somewhere in between depending on the aluminum to gallium ratio. When there is more than 40 % aluminium in the composition the band gap is direct. By having a higher band gap, the shell is able to confine the electrons in the GaAs core. This confinement happens because it is energetically favorable for electrons to occupy the core and not the shell. Excitation recombination will therefore happen in the core without loosing energy to surface recombination. Since the shell contains aluminum it is subject to oxidation, this is negated by capping the shell in a thin layer of GaAs.

2.7.4 Excitation

When an electron gains energy above its normal resting place in the valence band it is said to be in an excited state. This happens when the electron absorbs a photon. When the incoming photon transfers more energy to the electron than the energy gap between the VB and CB, an electron-hole pair is created. An electron in the VB gets temporarily excited to the CB, this leaves behind a vacant orbital. This absence of an electron means that an atom in the VB is positively charged, the cloud of electrons in the valence band can still move about, even into the vacancy created by the departed electron [32]. However, as long as the electron is in the CB, there will be a *hole* in the VB. Holes are quasiparticles with an equal, but opposite charge of the electrons, i.e. positive charge. They behave in much the same way electrons do, and even have an *effective mass* [59]. However, since the movement of a hole is actually the movement of several electrons, the hole has a lower mobility and a larger effective mass than the electron.

An *exciton* is a state where the electron in the CB is bound to the hole, i.e. to the electrons in the VB [60]. They are in a bound state, governed by the electrostatic Coulomb force between the free electron in the CB and the bound electrons in the VB. Excitons just like holes are quasiparticles. They do not have a net charge, but are still able to transport energy. There are several types of excitons, however, for most semiconductors the Wannier-Mott excitons are the relevant ones [61, 62]. The binding energy for these excitons is around 0.01 eV with lifetimes around 1 ns [63]. Excitons decay when the electron recombines with the hole. As long as the thermal energy, kT, is lower than 0.01 eV, which is the binding energy of the exciton, a photon may be emitted. This happens at low temperatures and replaces the free electron-hole recombination found at higher temperatures.

Excitons can be further classified as either free, bound, or bi-excitons [60, 64]. Free excitons have an electron-hole pair that is not bound, i.e. the exciton is free to move about in the crystal lattice. In a bound exciton the electron-hole pair is bound to a defect, such as a lattice atom vacancy. This binding increases the coulomb energy, this in turn decreases the energy available for the bound exciton. The bound exciton has lower energy than that of the free exciton. The biexciton is, as its name suggests, formed of two excitons. When

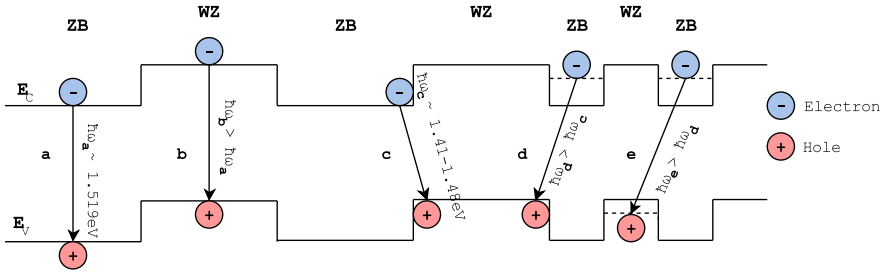

Figure 5: Different types of transitions that may occur in GaAs. Type-I transitions, **a** and **b** [65], are when the electron travels from ZB to ZB or WZ to WZ respectively. Type-II transitions, **c** [66], manifests when the electron in ZB recombines to the hole in WZ. If there are stacking faults in the NW, formation of quantum wells might occur, these have discrete energy levels indicated by dashed lines. This makes transitions **d** and **e** possible. $\hbar\omega$ represents the energy of released photons at 0 K.

the biexciton recombines, it disintegrates into a free exciton and a photon. The energy in the photon is lower than that of the exction because of the binding energy between the two excitons.

2.7.5 Band transitions

The electronic properties of GaAs ZB and WZ NWs are similar. The difference between the band gaps have been reported to be in the area of 29-35 meV at 0 K [65, 67] with a valence band offset at about 100 meV [66]. Even if the precise value of the band gap in WZ NWs is not agreed upon, it is accepted that it has a band gap higher than that of ZB NWs. If a nanowire experiences stacking faults, i.e. ZB and WZ interchanging, there may be additional transitions. In figure 5 these transitions are illustrated. As can be seen, **a** and **b** describes the transition from CB to VB within the same crystal structure, i.e. type-I transitions. ZB nanowires are expected to emit a photon with an energy of about 1.519 eV. WZ NWs will according to prior research emit at an energy of about 1.548-1.554 eV. Transitions occurring from one crystal structure to the other in the same NW are defined as type-II transitions. The energy of the emitted photons in type-II transitions is around 1.41-1.48 eV [66]. All of these energies are at 0 K.

Stacking faults in the NW opens up possibilities for further transition types. Quantum wells may form and transitions from discrete energy levels within these quantum wells are possible. **d** and **e** in figure 5 shows two possible scenarios.

2.7.6 Temperature dependence

Semiconductors are sensitive to temperature changes. The band gap energy, E_g, will normally decrease for increased temperatures. At low temperatures, E_g is non-linear. This stems from the temperature dependent dilation of the lattice [68]. At high temperatures, however, this dilation effect is linear with the temperature and only accounts for about 25

% of the total variation in E_g [69]. At high temperatures the major contribution comes from a shift in the relative position of the VB and CB due to a temperature-dependent electron lattice interaction.

High temperatures are defined as those exceeding the *Debye temperature* [70]. The shift in the band gap is temperature dependent in the following way

$$\begin{aligned} \Delta E_g &\propto T^2, \qquad T \ll \theta \\ \Delta E_g &\propto T, \qquad T \gg \theta \end{aligned} \tag{1}$$

where θ is the Debye temperature, T is the temperature and E_g is the band gap energy. In 1967 Y. P. Varshni used empirical data to create what is now known as the Varshni equation [69].

$$E_g(T) = E_g(0) - \alpha T^2/(T+\beta) \tag{2}$$

This equation uses three parameters, $E_g(0)$, α, and β to estimate the band gap at a given temperature. Where $E_g(0)$ is the band gap at 0 K, and α and β are material constants with units eV/K^3 and K^3 respectively. This equation describes the previous mentioned temperature dependence of semiconductors.

In 1991 O'Donnell published a paper [71] explaining an equation for the temperature dependency,

$$E_g(T) = E_g(0) - S\langle\hbar\omega\rangle[\coth(\frac{\langle\hbar\omega\rangle}{2kT}) - 1] \tag{3}$$

that is designed to have a better fit to measured values. $E_g(0)$ is the band gap at 0 K, S is a dimensionless coupling constant, and $\langle\hbar\omega\rangle$ is the average phonon energy. This equation is, as the Varshni equation, deduced by looking at empirical evidence. Varshni's equation is included on the basis that it is still widely used.

2.7.7 Interactions reducing photon emission

Aside from temperature, there are several causes of reduced photon emission in a NW at the desired energy. Several types of interactions emits a photon, however, not with the expected energy and they are therefore not useful for the intended purpose of the NW.

Bound excitons is one factor reducing photon emission. By travelling via defect levels the electron-hole pair can either recombine without emitting a photon or emit a photon with an energy lower than the band gap energy. If no photon is emitted the energy lost by the electron can be emitted as a phonon [72].

Stacking faults can also reduce photon emission in various ways [73]. If quantum wells are formed, the energy released by recombining exciton will not match the energy released in the free exciton. This can lead to separate energy peaks if there are enough SFs, or to a broadening of the peaks.

2.8 Photoluminescence

Photoluminescence (PL) is light emission in any form after the absorption of photons. By use of PL; the band gap, carrier lifetimes, mobility and several other properties [74] can be found. The fact that PL is a non-destructive and highly sensitive process makes it attractive. The different photon emission situations are illustrated in figure 6.

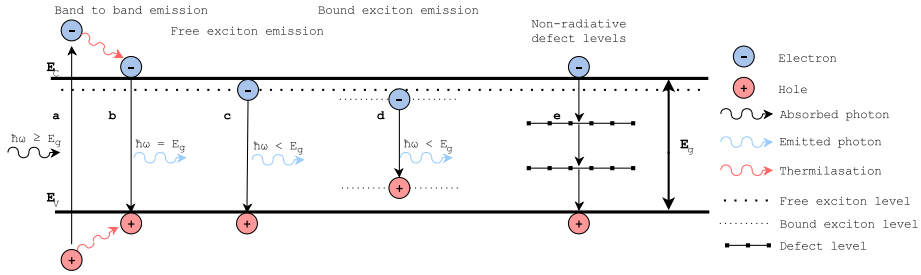

Figure 6: Absorption and emission of photons in a semiconductor. E_C is the conduction band edge, E_V is the valence band edge and $\hbar\omega$ is the emitted photon energy. **a** electrons in the valence band get additional energy from absorbed photons and are promoted to the conduction band. **b**, **c**, **d** when recombining with holes they may radiate photons. **e** it is also possible for electrons to loose their energy without radiating photons.

An incoming photon is absorbed by the material. This is illustrated by **a** in figure 6. If $\hbar\omega \geq E_g$ the incoming photon may promote the electron into the conduction band. The incoming photon may even have enough energy to excite the electron well up into the CB. This extra energy exceeding the band gap is normally wasted. Thermalization, which is the collisions with other electrons and interaction with phonons, will relax electron energy and the electron will be left at the CB edge. This may also happen to an electron deep in the VB, it may be excited and leave a hole in its place. This hole will undergo thermalization and end up at the VB edge. This process happens in the femtosecond regime for both electrons and holes [49].

Band to band recombination as depicted in figure

Step **c** in figure 6 shows the free exciton emission. The photons radiated in this process has $\hbar\omega < E_g$. At low temperatures, the free exciton emission is dominating. Step **d** describes the bound exciton emission. It has an energy lower than that of the free exciton, and therefore emits a photon with less energy. Both the free and the bound exciton recombine in the order of nanoseconds [63].

If there are defect levels present in the material, non-radiative recombination is possible. This is a process where the jumps in energy are small enough that energy is released in the form of phonons instead of photons. Defect levels can in addition to non-radiative transitions have radiative transitions. The emitted photon will have an energy lower than the band gap energy.

In figure 5 type-II transitions are shown. These emit photons with $\hbar\omega < E_g$.

2.8.1 High intensity PL

At high intensities of incoming light further transitions may occur, a situation called band filling can occur. Figure 6 is limited in that it does not show everything that can happen at high intensities. This is because the band gap is formed as explained in section 2.7.2. When the intensity is high, i.e. a high amount of incoming photons with $\hbar\omega > E_g$, the bands in centre of the band gap will be filled. In figure 7 the high intensity situation is

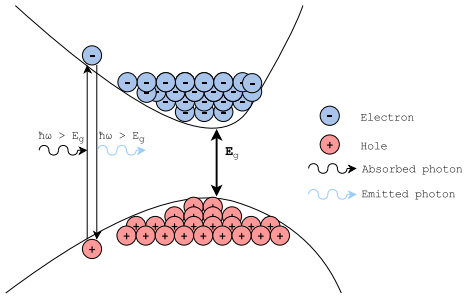

Figure 7: High intensity situation where an incoming photon excites an electron. The energies close to the band gap is continuously filled, meaning some electrons will be left at higher energies until they recombine. When recombining, the emitted photon will have an energy higher than the band gap.

illustrated. Some excited electrons will not get the chance to thermalize all the way to the band edge, because of the constant creation of new excitons taking up the states closest to the band edge. This leaves these electrons at higher energies until they recombine with their hole giving a photon with energy $\hbar\omega > E_g$. However, in opposition to this effect is the band gap renormalization (BGR) effect [75]. BGR decreases the band gap energy with increasing carrier density, i.e. with increasing amount of electrons excited into the CB. This happens due to electron-electron and electron-ion interaction.

3 Experimental

3.1 Substrate preparation

All but one of the samples with nanowires presented in this study are grown on patterned Si(111)B substrates, whereas the last is grown on an unpatterned Si(111)B substrate. By patterning the substrates a thin oxide film is left with holes through the oxide where the Si is exposed. Ga will nucleate on the substrate of the Si and not on the oxide. For this study different methods of patterning these substrates have been used prior to growth of NWs. Namely EBL and NIL. Both substrate patterning techniques are carried out with the intention of creating the same pattern. This pattern is illustrated in figure 8. For EBL the pattern on the samples included in this study is made in a 500 μm $\times$ 500 μm area since this is a slow process. As seen in the figure there is a 1 μm pitch and a hole size of 100 nm. Much can be said about the techniques used to achieve these patterns, however, in this study only the results from the patterning will be discussed.

The process for both EBL and NIL is similar. First the substrate is patterned using one of these techniques as described in chapters 2.5.1 and 2.5.2. This leaves a layer of resist on top of the oxide covering the sample. To create the holes in the oxide the sample is etched. This etching can be done by various etching techniques, however one commonly used technique is reactive ion etch [76].

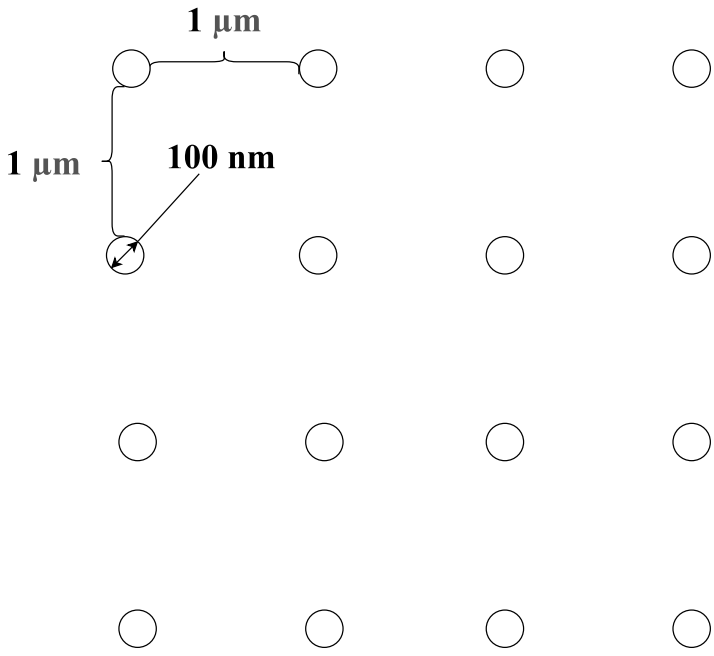

Figure 8: The patterning used for all patterned samples in this study, the oxide layer is 40 nm thick.

Wafers are normally patterned in a batch operation. This means there is often some time between the patterning and growth. Unless the substrates are kept in vacuum from the moment they are patterned until they are grown a native oxide will build up from oxygen. Depending on how much exposure the substrates are subjected to, the supposedly naked substrate in the holes may have a layer of oxide on it. Because of this an additional etching step is needed before MBE growth. This etch is done with a 1% hydrogen fluoride HF solution. This is a wet etch which is isotropic. In figure 9 an example of what the hole ideally should look like and what it actually looks like after etching is shown. The wet etch is used because it is easy to perform, and cheap. It is possible to achieve a closer resemblance to the ideal etch with more expensive and time consuming tools.

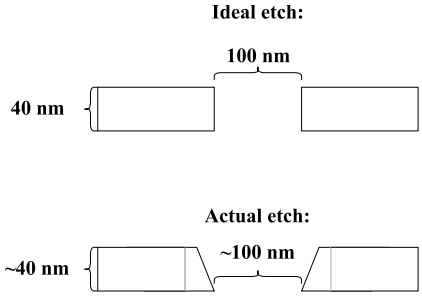

Figure 9: The ideal and actual holes after etching with isotropic wet etch.

In figure 10 scanning electron microscopy (SEM) images of an unpatterend and a patterned growth is shown from the top down perspective. Both of these samples are grown at the same time. It is obvious from the figure that on the unpatterned sample there is a fair amount of 2D growth, whereas on the patterned sample there is less. Because the unpatterned surface allows Ga nucleation anywhere, it is possible for a thin-film to form. As seen in the figure, only some locations have nanowires, however the rest of the surface grows with added materials. For a patterned wafer, this is not the case. Since there will be no growth on the oxide and only in the holes. The 2D growths that happen on the patterned sample is because NWs do not grow in the right direction, or when the droplet does not form a NW. It can be seen in figure 10b, where the growths along the surface looks like nanowires. The sizes of the nanowires seen in the unpatterned sample is variable, some thick and some thin, in the patterned growth the sizes seem more uniform. However, this is not a fair comparison of unpatterned vs patterned growth. This is because the growth conditions has been optimized for uniformity in growing the patterned nanowires in this case. Because Ga can nucleate anywhere on the unpatterned substrate there is a difference in the III/V ratio experienced by the samples.

3.2 Growth

Using MBE the samples are grown with the parameters shown in figure 11. The arrows in the figure show the processing path for each sample, where the shared boxes is a process that is applied to all samples with arrows pointing to them. Furthermore some details

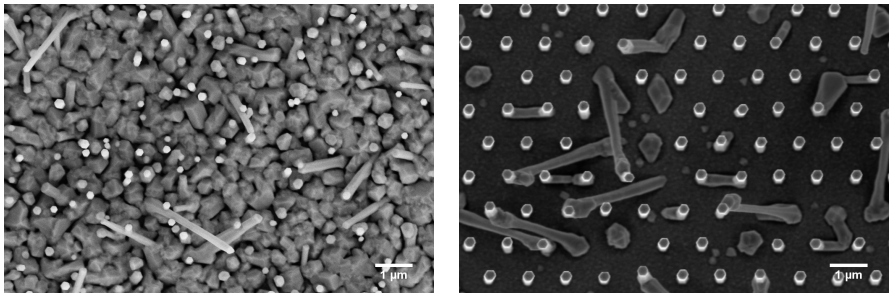

(a) SC490R (b) SC490

Figure 10: High resolution SEM images of one of SC490R and SC490. SC490R on a an unpatterned substrate and SC490 on a patterned substrate. The image is taken top down where the bright spots are individual nanowires.

that applied to all samples is written above the samples. The MBE growth is divided into several processes.

The prepared substrate is etched before inserting it into the MBE to remove native oxide buildup. This is done with a 1 % solution of hydrofluoric acid and a 12 second O_2 plasma. The acid bath time depends on how much exposure to oxygen the sample has been exposed to.

Once the sample is inside the MBE it is first heated up to 625 °C. Once the sample has reached this temperature Ga predeposition begins. This step is where the droplets nucleates in the patterned holes.

After the droplet is formed the actual GaAs core growth is started. To ensure that the growth has the optimal starting conditions, the first minute of growth is done with the optimized As flux of 3.1E-6. Following this the desired As flux is selected for the rest of the core growth. The temperature is still kept at 625 °C. The growth rate is governed by the As flux, for this study all samples are grown with 0.7 ML/s of Ga.

Some samples have an axial AlGaAs section grown on them after core growth. This is done in an effort to avoid stacking faults that can often be found in the tip of the nanowires. This is a slow and short growth, 5 minutes with 0.15 ML/s of aluminum and 0.3 ML/s of Ga.

Next the droplet is solidified to prevent further axial growth, this typically takes 12-15 minutes. Depending on the growth rate controlling material, the droplet is solidified by stopping the flow of either Ga or As. At this point the structure where the desired PL signal is generated is done. However, because of surface recombinations as mentioned in chapter 2.7.3 a passivation layer is required.

Each nanowire is passivated by encapsulating it in an AlGaAs shell. This has been grown at different temperatures, 460 - 630 °C, in an effort to rule out some undesired effects seen in the PL spectra. Shell growth is radial because the droplet is solidified, with a similar slow growth as seen in the axial insert, 0.1-0.15 ML/s of aluminum and 0.2-0.3 ML/s of Ga. The shell growth process takes 20 to 30 minutes.

To stop oxidation in the aluminum of the shell a capping is grown as a last step. This consists of GaAs and is grown at the same temperature as the shell with the same growth

rate of Ga, 0.2-0.3 ML/s. The capping is a thin layer of material which is grown radially for 8 minutes.

From table 1 and figure 11 it looks as if SC542 and SC549 are identical. The growth parameters are identcial, and the patterning method is. However, due to surface oxidation SC542 had a very low yield and a substrate that had less exposure to air was chosen so that the sample could be regrown.

Table 1: Key differences in growth parameters for all the nanowires included in this study.

Sample	Patterning	As flux [E-6]	Core growth [min]	Shell growth [°C]	Axial insert
SC343	Old NIL	5.5[a]	25	630	Yes
SC490R	-	3.1	32	460	No
SC490	EBL	3.1	32	460	No
SC506	New NIL	4	29	460	No
SC532	Old NIL	3.1	31	625	Yes
SC535	EBL	2	48	460	No
SC542	EBL	4	26	625	Yes
SC549	EBL	4	26	625	Yes

a Was grown with an old MBE setup, flux is not comparable to new growths.

3.3 Sample preparation

3.3.1 Dispersion for measuring individual nanowires

To be able to measure the PL spectra of an individual nanowire it is necessary to disperse the as grown sample. To achieve this a simple method is used.

A transmission electrom microscope (TEM) grid made from silicon nitride (SiN) is used as the film where the nanowires are deposited. A TEM grid is a thin silicon substrate with holes etch through it. This substrate is coated with a thin film of nitride, this creates a window effect. Samples that are to be studied can be placed on these windows where there is no silicon and only nitride. This substrate is chosen because it will not interfere with the PL signal from the nanowires, and more importantly makes it possible to do TEM studies of the samples at a later point. Furthermore, because this TEM grid has an orientation, it makes it easy to find and label individual nanowires, which makes it possible to measure a specific nanowire several times at separate occasions. An illustration of a TEM grid is shown in figure 12. The lighter colored sections is where there is no silicon and only a nitride film, these sections are referred to as windows and they are also where the measured nanowries are located.

The as grown sample containing the NWs is scratched with a scriber, this breaks nanowires off from the substrate. To transfer the wires that have broken free, a small droplet of isopropanol is placed on the tip of a sharp object. This makes it easier to place the droplet where desired. The droplet is placed on the sample, after which the TEM grid is placed facing down into the sample with the droplet. The droplet is then given time to evaporate while the sample and TEM grid are laying together, after which the sample is removed from the TEM grid. After evaporation, there is a variable amount of nanowires

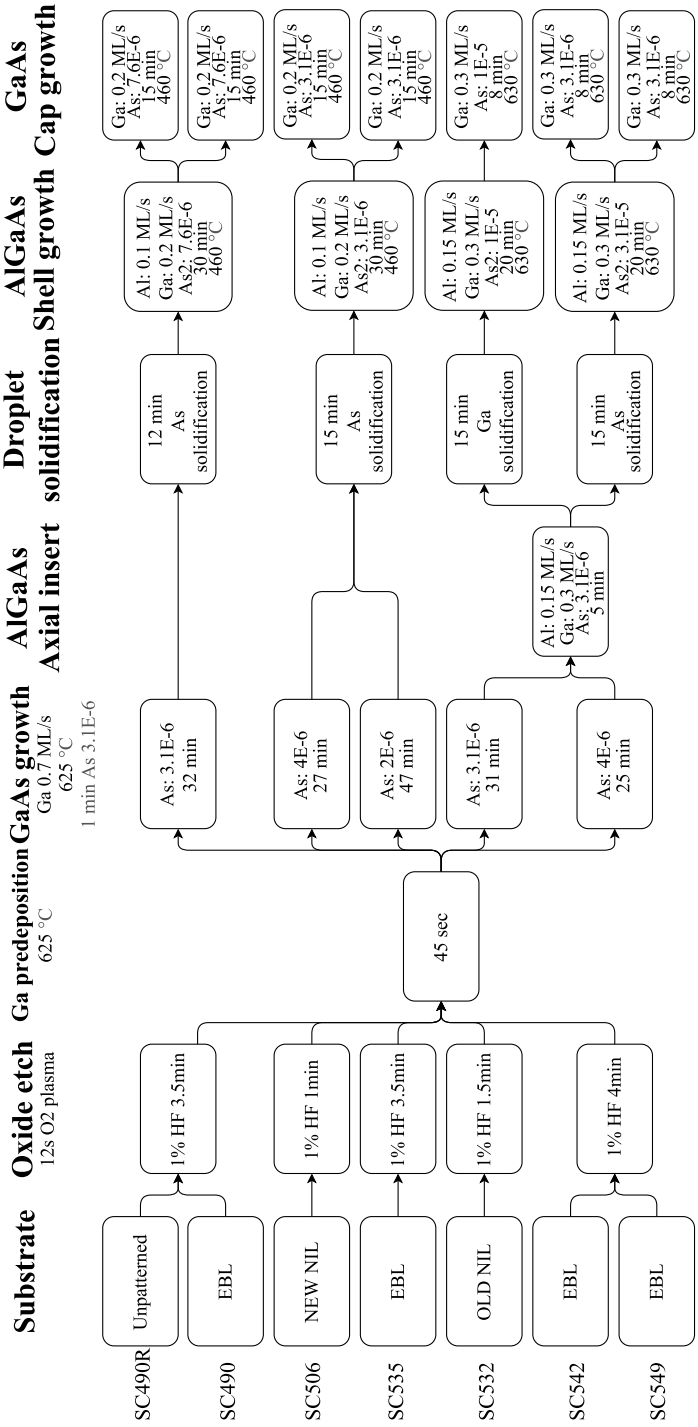

Figure 11: A diagram showing the complete growth process for all samples in this study. Arrows leads to the next step. Several arrows pointing to the same box means that these samples shared this step. Some parameters that were constant is shown above process steps.

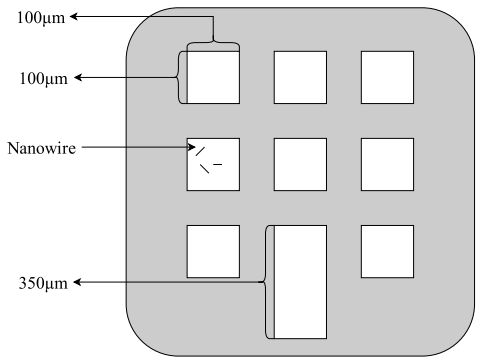

Figure 12: SiN TEM grid used to facilitate measuring of individual nanowires.

randomly scattered across the TEM grid. It is desirable to not have an abundance of nanowires because it means that there is only contribution from one nanowire when exposed to light. Furthermore, if the nanowires are broken at the base it is better. This is because if the NW is broken in the middle, the resulting PL spectra may not be representative since the difference in crystal structure within the nanowire can be localized to the part that is broken off.

Once the isopropanol is evaporated the TEM grids are inspected in an optical microscope at first to ensure the right density nanowires is achieved, and later SEM. From the SEM pictures, the nanowires that fit the criteria are labeled. I.e. single NWs that have sufficient space around them and are mostly complete. Figure 13 shows an example of how one window on the finished TEM grid with nanowires can look. As is evident from the image there are both suitable and unsuitable nanowires. Every location with several NWs on top of each other is unsuitable.

3.4 Measurement setup

The PL setup is illustrated in figure 14. This section will describe the instruments used.

I The laser used is a 4.3 mW, 532 nm laser diode. That means the laser emits photons with an energy of 2.33 eV, which is much larger than the band gap for GaAs. This allows the photons to excite more states in the NWs, as explained in section 2.8.1.

II Variable filter, that, depending on its state allows part of the light through. This is used to achieve the desired power from the laser during measurement.

III Filter removing undesired wavelengths from the beam. Wavelengths around 532 nm, are allowed to pass through. Other wavelength components generated by the laser are removed from the transmitted beam.

IV The beam splitter transmits part of the laser power to the sample. Part of the emitted light from the sample is also passed through on its way to the detector. A normal mirror can not be used here since light needs go through for some directions.

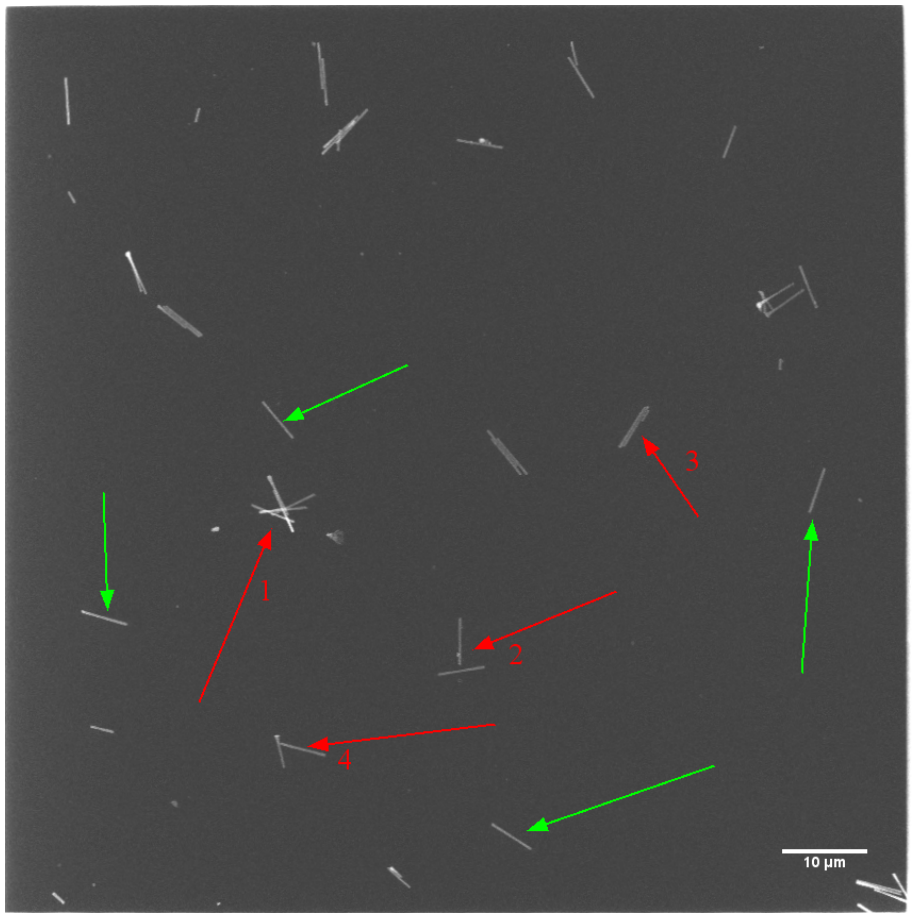

Figure 13: An SEM image from a TEM grid window showing the individual NWs. Some examples of accepted and rejected NWs are shown. The green arrows point to NWs that can be used for PL measurements. The red arrows point to unsuitable NWs. Number 1, and 3 is unsuitable because there are too many NWs clustered together. Number 2, and 4 are undesired because they are too close to other nanowires, meaning the emitted signal may be from both wires pictured.

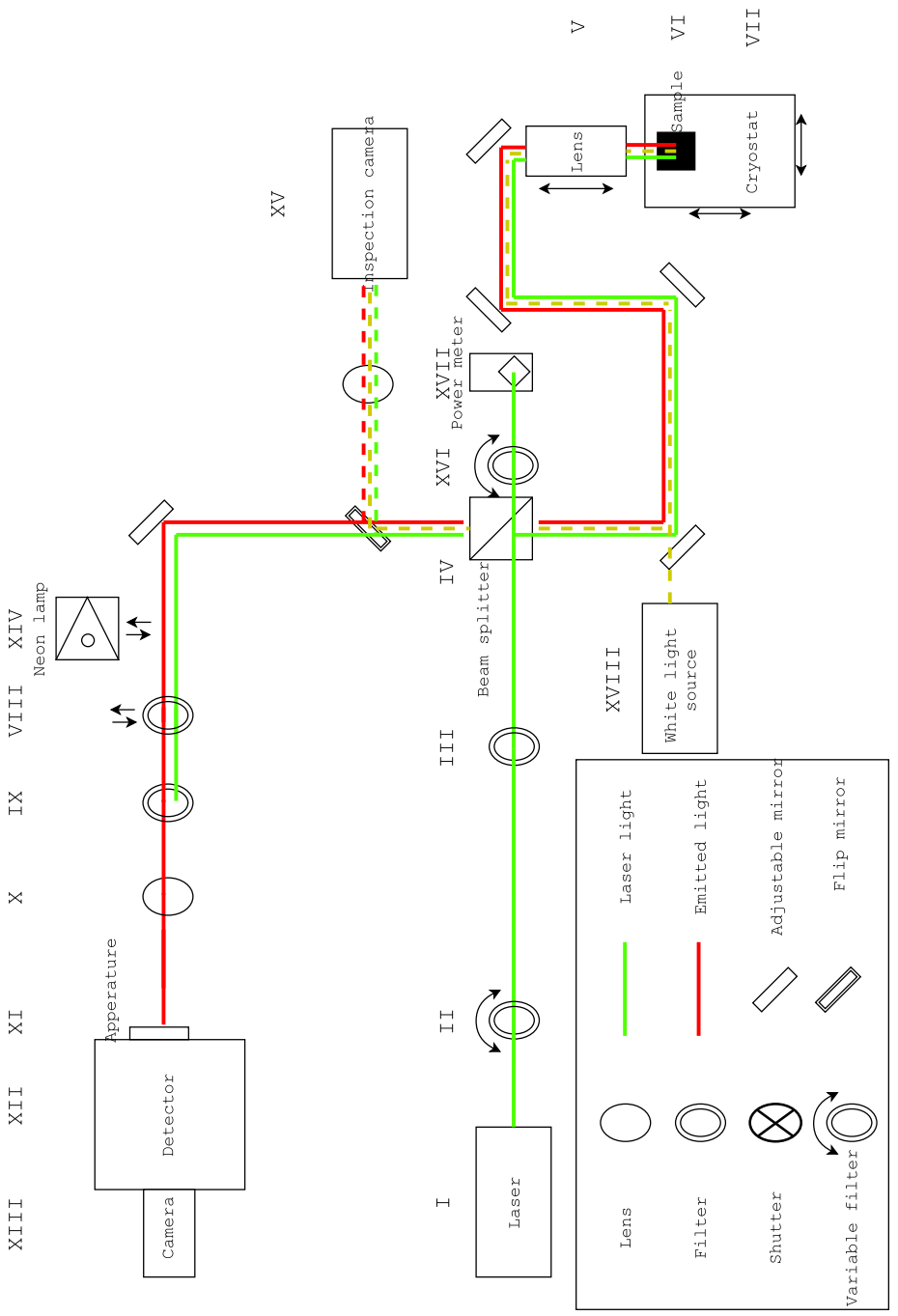

Figure 14: The setup used to excite and measure samples. A laser generates light at a given intensity, this is focused on a very small spot, 1-2 μm, on the sample. Photons emitted from the sample are focused into the detector and attached camera.

V High quality objective, *50X Mitutoyo Plan Apo NIR HR*. This is attached to a variable position mount. This allows for movement in only the z-direction. That means it can be used to focus the beam onto the sample. This lens also collimates the light coming from the sample. By using this objective it is possible to have a spot size of about 1-2 μm for the incoming 532 nm laser. The spotsize is assumed to be 1.5 μm.

VI The sample is placed in a cryostat mounted on a variable position mount. The sample can be moved in the xy-directions. This is done to make it possible to hit the desired location on the sample with the focused light, but also to allow for measurements of different positions on the sample.

VII Cryostat, *Cryocool-G2B, Cryo industries*. This is connected to a temperature controlling unit, *Lakeshore 336*. This system lets the user select the desired temperature for the sample. By applying vacuum and helium it is possible to control the temperature in the range of 11-325 K.

VIII Filter, *Thorlabs, NE240B, optical density: 4.0*, used to reduce intensity of all wavelengths of the output signal from the sample. This is removable and only used to avoid saturation.

IX Filter removing all wavelengths below a given value, ensures no laser light and only the emitted light reaches the detector. The filter removes wavelengths below 650 nm.

X Lens focusing the beam onto the spectrometer entrance slit.

XI The first part of the detector that light reaches is the entrance slit. The light that enters the spectrometer then reaches a shutter which allows different exposure times to be set. By lengthening the exposure time it is possible to detect signals in low-intensity conditions.

XII *Andor SR-303i-B* is a spectrograph connected to a computer. The spectrograph separates the light into a frequency spectrum. This is done by sending the light through a diffraction grating, the light coming out of this grating will be separated in distance for different wavelengths much in the same way a prism separates wavelengths. By shining this separated light on the connected camera, it is possible to measure the number of photons with a given wavelength that hits the CCD camera and send the results to the computer.

XIII *Andor DU401A-BR-DD* is a spectroscopy CCD camera able to measure low-light conditions from the UV through to the near IR range. A CCD camera works by having several photoactive regions that accumulates electric charge proportional to the intensity at that location. Since the beam is split into different wavelengths spatially, it is possible to know where specific wavelengths hits the camera.

XIV Removable neon lamp, *SP200V, Electro-Technic, inc.*. The neon lamp emits light in the red to infrared region and has known intensity peaks for various wavelengths, this is used as a reference for calibrating the wavelength spectra measured by the detector.

XV Camera, *WAT-202D*, connected to a screen can be used to make sure that the light is focused and that it is hitting the sample where desired. By using a flip mirror this is only enabled when needed. A lens focuses the image and ensures that the whole beam is in view on the screen.

XVI Variable filter, that, depending on its state allows part of the light through. This is calibrated so that the same power is observed by the power meter, as the power that hits the sample.

XVII Power meter, measures the power of the laser. This meter is used for every measurement to ensure correct excitation power.

XVIII White light generator is used to shine light on the sample, this in turn is reflected back into the camera connected to a screen giving a magnified view of the sample used for inspection, focusing the beam, and finding individual nanowires for measuring.

Using this setup it is possible to measure individual NWs after they have been dispersed onto a TEM grid. The exact size of the beam spot is difficult to estimate, furthermore, what part of each NW that gives rise to excitation is hard to say. This means that measurements done with this setups inherently have some uncertainties.

3.5 Cooling samples

Because the free exciton peak can only be found for low temperatures it is necessary to cool the sample down. Furthermore, cooling the sample reduces thermalization. This means that a stronger emission can be measured from a cooled sample. The cooling system uses helium (He) gas as a coolant. A water cooled compressor circulates and cools the He gas in the system. Below 5 K helium can condense, to avoid this, the cryostat has heater elements, one of these is set to keep the temperature at a minimum of 5 K to avoid condensation. By the time the helium reaches the sample mount in the cryostat it has heated up, this is the reason measurements are done at 12 K. It is not possible to get the sample mount lower than 12 K with this setup.

3.6 PL measurements

The photoluminescence spectroscopy measurements are done in a way to minimize ambient noise. This means covering or removing all light sources. The sample is cooled down using the cryostat to the desired temperature. After cooling, a suitable area on the sample to perform measurements is found. The incoming laser is then focused using both the real-time results from the spectroscopy unit and by using the inspection camera. This ensures that the emitted signal is at its strongest and that the focus is on the nanowires. This setup does not measure individual nanowires when they are placed in an array, the focused laser then covers several NWs. This means that a variable number of nanowires is measured for each sample, meaning a direct comparison of emitted power between samples is not possible. However, by measuring at several locations for each sample, it is ensured that the energy of the emitted photons is not dependent on the location of measurement. With dispersed NWs it is possible to measure individual NWs as well, as explained in section

3.3.1.

To ensure that the measured position is not an anomaly, several locations are measured and compared. In an ideal world with a 100 % yield for all samples this would not have had the same importance, however, for real samples there might be locations with faults and it is a necessity to measure several locations. Furthermore, even if the yield was 100 %, it is not possible to see individual nanowires when measuring as grown samples with this setup. This means that there is a potential for measuring a variable amount of nanowires as shown in figure 15. This example shows an idealized beam spot. In reality the beam spot will not be focused entirely in one area but will have a Gaussian distribution, which means that the center will have a higher power density than the outskirts.

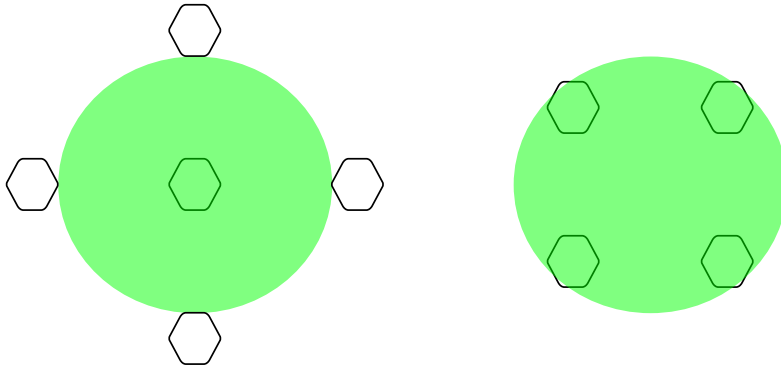

(a) (b)

Figure 15: Two situations that might arise when measuring nanowires with the setup used in this study. The octagonal shapes represent nanowires, and the green circle represents the beam spot.

For measuring the sample with varying temperature, the temperature and laser power variations subjected to each sample is comparable within that sample. There is no movement done on the sample until all measurements are done. However, for each new temperature measured, the focus is adjusted. This is done because during temperature change, the sample will undergo thermal contraction or expansion [2] changing where the focus on the sample is. By waiting until the temperature is stable in the sample and then adjusting focus, the maximum amount of emitted photons with the desired wavelength is emitted.

Samples with a very high excitation requires an additional filter to reduce the output before it reaches the CCD camera to avoid saturation.

3.7 Measurement method

3.7.1 Calculating integrated intensity

To calculate the integrated intensity it is important to know the exposure time and any frequency dependent filters used. One such filter is show as XVIII in figure 14, this filter

is frequency dependent. To account for this, the integrated intensity was adjusted in post processing to the value of the absorption in such a way that the measured intensity at the CCD would look like it never passed through the filter. In addition to accounting for the filter used, the shutter does not open and close at an arbitrarily fast speed. Although the software accompanying the shutter allows the user to select exposure times down to $1 * 10^{-5}$, after calibration this proves to not be true and a realistic exposure speed at its lowest is $2 * 10^{-2}$. Furthermore, because there is always some background noise which might be variable, it is necessary to remove this background nose from the measured intensity. After this background noise has been removed there should only be a signal from the sample. This can then be integrated and divided by the exposure time to find a integrated intensity per second L_e.

3.8 Analysing results

To analyze the results Python code was written. In this code the results are imported, along with the reference measurement done with the neon lamp. This is used to calibrate the wavelength difference between the measurements and actual values. Filter VIII from chapter 3.4 is also accounted for by using data distributed by the manufacturer. The final calibration is adjusting the exposure time. Since the spectrograph allows the user to set exposure times that are shorter than the shutter can open an close, the exposure time can be wrong as seen in chapter 3.7.1. Having done these calibrations, the data can now readily be exported in any way necessary.

4 Results

4.1 Growth

In figure 11 the complete list of growth parameters for all the samples measured can be found. While in table 1 the key differences between them are highlighted. The purpose behind SC532 was to make an identical sample to SC343, SC343 is a sample that has been measured previously that had good optical qualities. The sample results are included here as a reference.

Figures 16 and 17 shows SEM images from all the samples that are analyzed. Figure 16 shows SC343, along with the random growth sample, the 2D film growth is seen clearly on SC490R, as well as the large variation in NW physical properties. Figure 17 shows an SEM image from each patterned sample, compared to the random growth the nanowires for each sample are much more uniform. SC490 (a) has what appears to be the best nanowires in terms of physical uniformity and desired physical properites. This is as expected, since the growth had been optimized for the physical characteristics and yield for this growth. In table 2 the results of the physical properties have been summarized. From this table it can be seen that SC490 is the longest, and most uniform nanowire, with the highest yield out of all the measured NWs.

SC549 looks similar to SC490, however, the droplet is larger for some nanowires and the nanowires are tapered for SC549. This is again backed up by the results in table 2 where SC549 has a slightly higher variance than SC490, but still lower than all other samples. Some samples have a low yield, especially SC542. This is illustrated in the SEM image (e) where there are many missing or laying NWs.

Looking at table 1 and 2 there does not appear to be much correlation between As flux or patterning, and length/thickness of the NWs. However, for SC535 with the lowest As flux, the nanowires ended up anti-tapered.

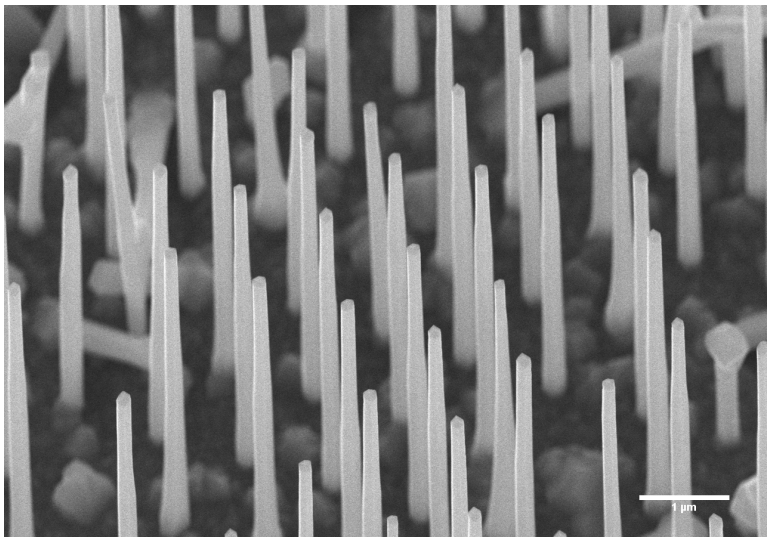

(a) SC343

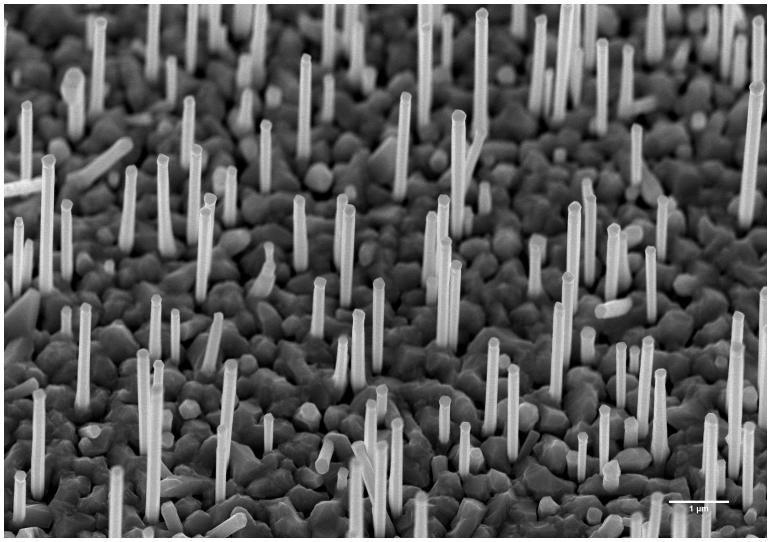

(b) SC490R

Figure 16: High resolution scanning electron microscopy image of the random growth sample analyzed in this report. This SEM image is taken at a 30°angle, which means that the scale bar is correct in the x-direction, but needs to be doubled in the y-direction.

Table 2: Nanowire physical characteristics after growth. Each averaged value represents a selection of minimum 40 nanowires. The yield is also given based on standing nanowires present among a selection of minimum 500 nanowires from each sample. The standard deviation is given as σ as a percentage of the averaged value. The top measurement of thickness does not take into account the droplet, and where the droplet is present is measured right below.

Sample	**Length** [μm]		**Thickness** [nm]				**Yield** [%]	**Shape**
			Base		**Top**			
	Avg	σ[%]	**Avg**	σ[%]	**Avg**	σ[%]		
SC343	5.7	6	271	13	151	8	59.3	Tapered
SC490R	2.3	40	193	16	173	13	-	Tapered
SC490	5.6	2	269	9	264	7	75.5	Hourglass
SC506	5.0	15	414	9	222	7	37.4	Tapered
SC532	3.6	13	274	16	220	18	49.3	Tapered
SC535	4.3	14	231	16	333	10	56.3	Anti-tapered
SC542	4.6	12	311	7	228	11	17.3	Tapered
SC549	4.6	5	280	7	204	11	37.9	Tapered

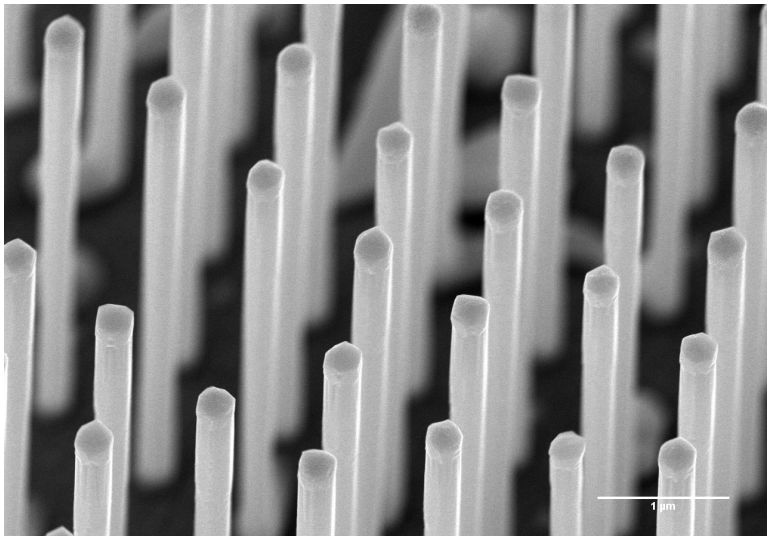

(a) SC490

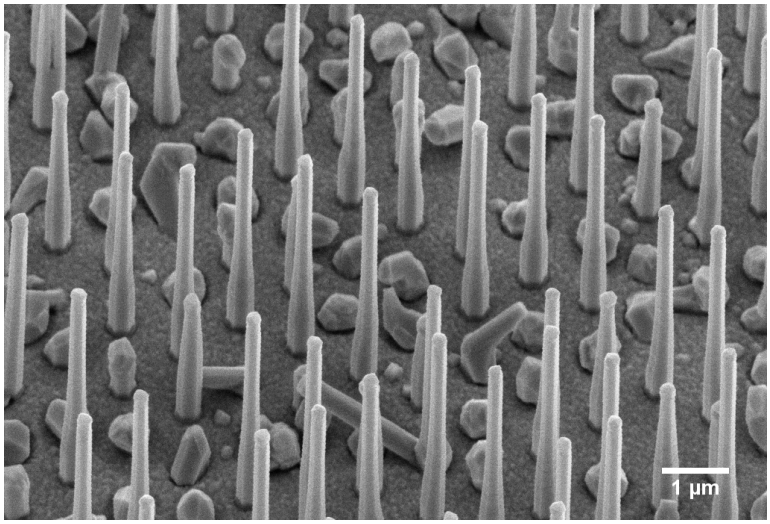

(b) SC506

Figure 17: High resolution scanning electron microscopy images of the as grown patterned samples analyzed in this study. The images are with different scale as can be seen on the scale bar. Furthermore, they are taken at a 30°angle, which means that the scale bar is correct in the x-direction but needs to be doubled in the y-direction.

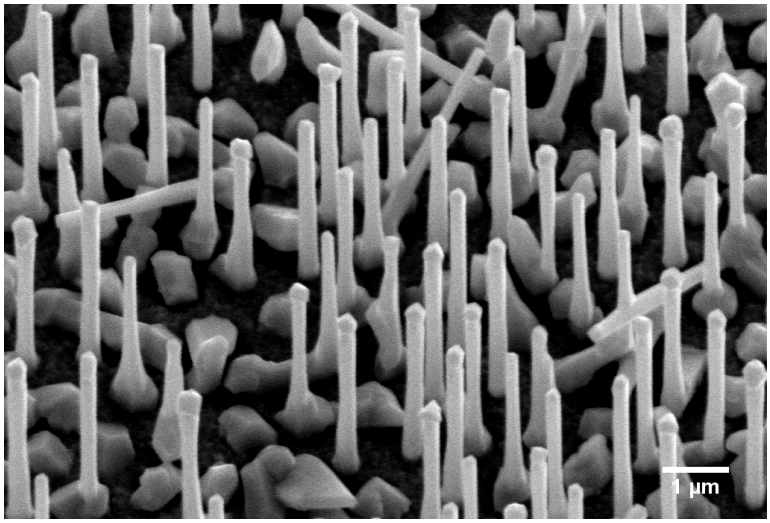

(c) SC532

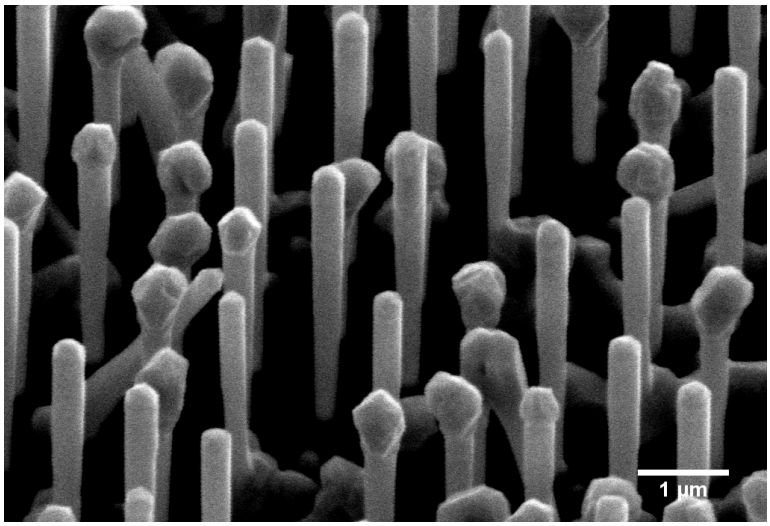

(d) SC535

Figure 17: High resolution scanning electron microscopy images of the as grown patterned samples analyzed in this study. The images are with different scale as can be seen on the scale bar. Furthermore, they are taken at a 30°angle, which means that the scale bar is correct in the x-direction but needs to be doubled in the y-direction.

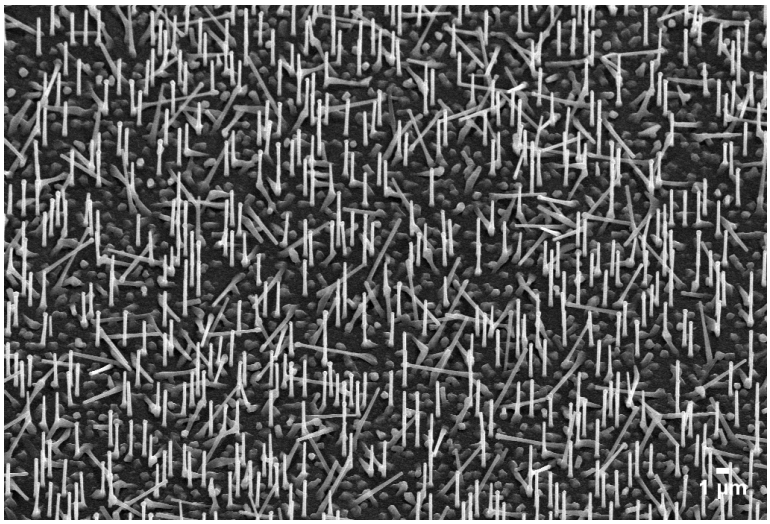

(e) SC542

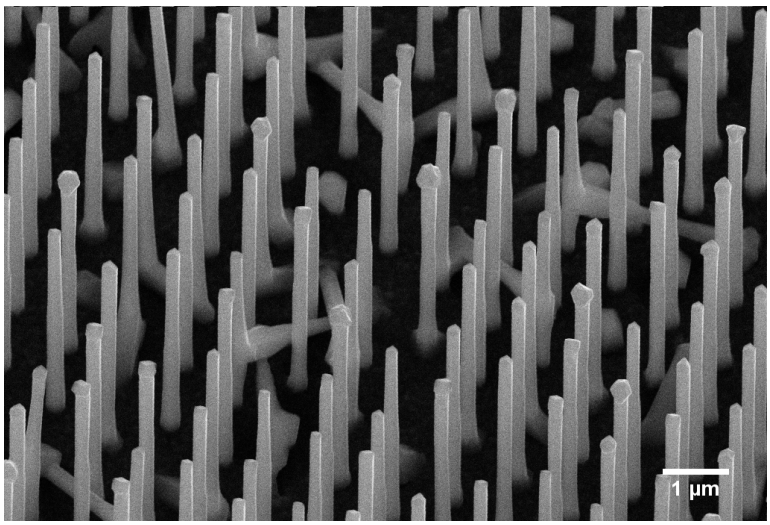

(f) SC549

Figure 17: High resolution scanning electron microscopy images of the as grown patterned samples analyzed in this study. The images are with different scale as can be seen on the scale bar. Furthermore, they are taken at a 30°angle, which means that the scale bar is correct in the x-direction but needs to be doubled in the y-direction.

4.2 Intensity

4.2.1 As grown measurements

Figure 18 shows how the integrated intensity per second is dependent on the power density on the sample. This result is also highly dependent upon where the focus of the beam is and how many nanowires are actually exposed to the beam as pointed out in section 3.6. Since this is averaged from at least four separate measurements, the results are comparable to some degree. However, it is not possible to compare accurately because of the nature of the measurement. Because of this, only the order of magnitude can be used a comparison. It is clear from the figure that there is some variation, even accounting for uncertainties. The sample with random growth shows an higher integrated intensity for all but the highest two power densities measured. Furthermore, all samples show a similar trend and increase in L_e for increased excitation power density. Other than the random growth sample, no sample shows an uncharacteristically high or low L_e. SC549 has a higher integrated intensity per second than SC542, this is logical since they are grown in the same way, and the major difference between them is the yield.

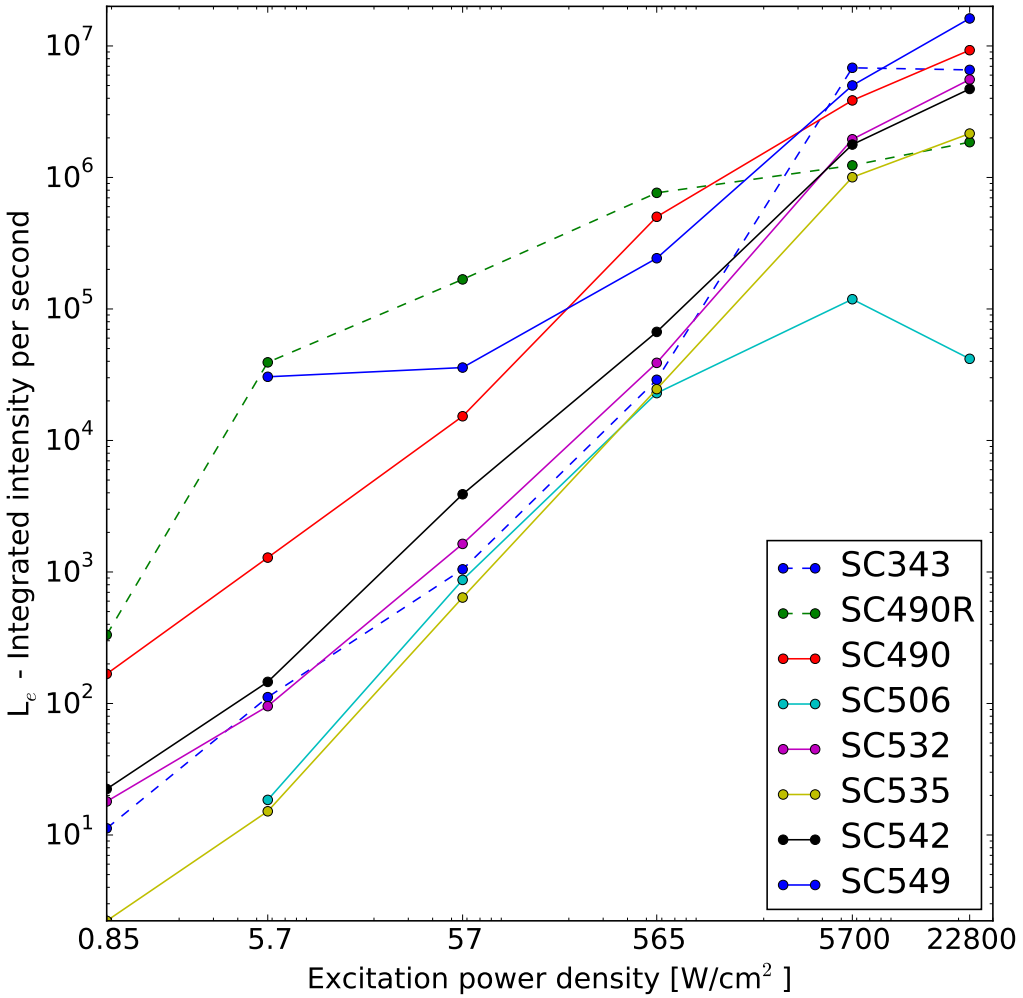

Figure 18: Logarithmic plot showing the average integrated intensity per second (L_e) on the as grown samples as a function of power density subjected to the sample, taken as the average of at least 4 different measurements at different locations on the substrate. Measurements were done at 12K.

4.2.2 Single nanowire measurements

Comparing the as grown measurements to the single nanowire measurements, L_e is lower, this is as expected since the as grown measurements include several NWs, and potentially some 2D structure at the substrate. It should also be noted that the random growth sample shows a lower L_e compared to the as grown measurements once it is measured as single nanowires. SC490R stills hows a stronger emission for low power densities, however, for the as grown measurements the integrated intensity per second from SC490R was 10 times larger than most other samples at low intensites. Where as in the single NW measurements it is 2 times larger. This likely has a great deal to do with the 2D film no longer being measured. Again the samples show little variance and behave in the same manner.

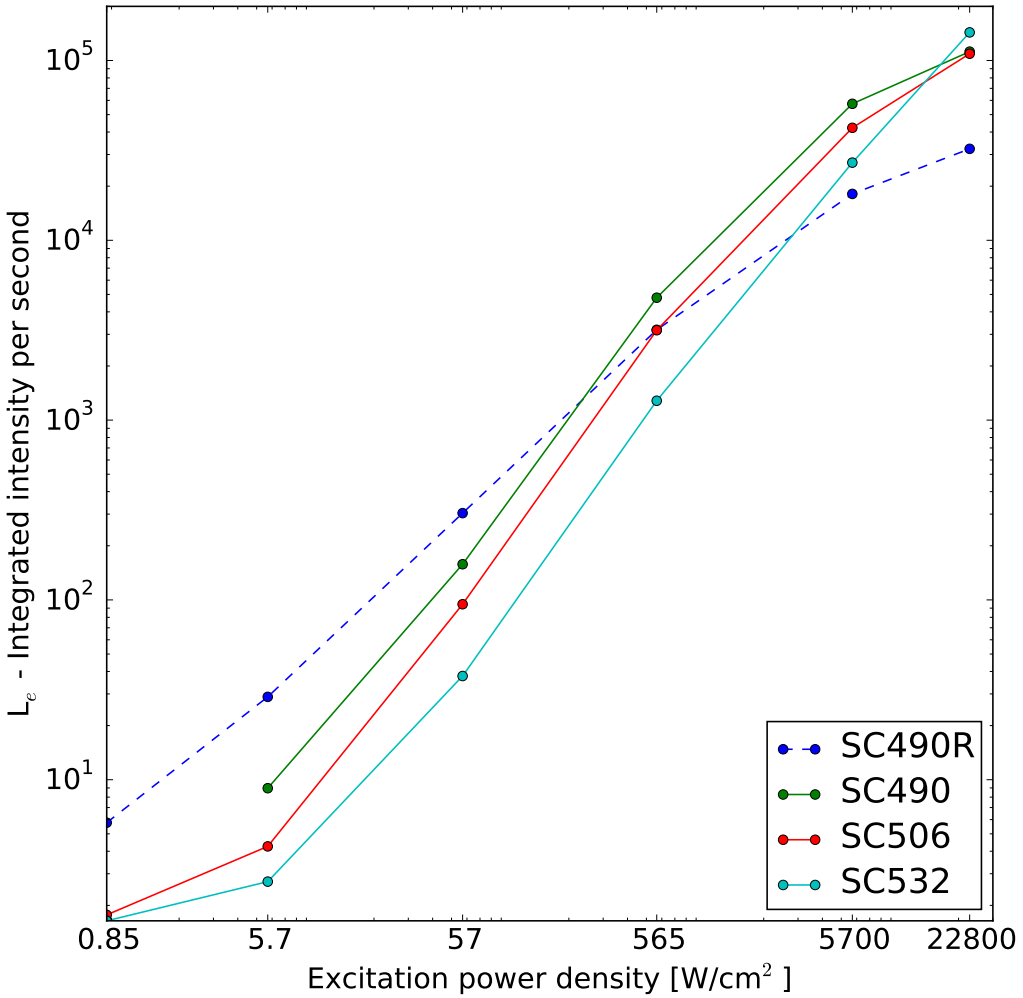

Figure 19: Logarithmic plot showing the average integrated intensity per second (L_e) for single nanowires as a function of power density subjected to the sample, taken as the average of at least 10 different measurements from at least 10 nanowires. Measurements were done at 12K.

4.3 Energy levels

4.3.1 As grown measurements

In figures 20 and 21 the as grown engery levels are presented for two different power densities. Only SC490 and SC490R show something that could be interpreted as the free exciton peak from the measured samples. SC343 which is the reference sample shows a clear free exciton peak. SC542 and SC549 are very similar nanowires as pointed out in chapter 3.2. This is reflected in their emission energy level which is very similar at just under 1.5 eV. For the reference sample, SC343, the free exciton emission can be seen at the high power density in figure 21. There is no clear answer as to why the emission peaks are located where they are. There does seem to be some correlation between growth rate and energy level in the case of SC535 compared to the rest. This sample was grown slower with the lowest As flux and also has a peak at the lowest energy, at just under 1.45 eV. For the higher As fluxes, there does not appear to be any correlation between As flux and energy level since SC506 has a lower energy level than SC532. Furthermore, the shell temperature growth does not appear to affect the energy level. For the axial insert it is hard to give any result since there is not enough different samples measured.

Figure 22 shows behavior that falls outside of the norm, where the focus is on any peaks observed between 1.4 and 1.55 eV. These high energy peaks, especially those around 1.84 eV have been observed in previous samples. However, for all the samples presented in this study, SC542 was the only sample with noticeable emission in this region. The highest power density did not get measure any emission in this region, however, for this measurement the filter (VIII) discussed in chapter 3.4 was used. Since the emission from the high energy peaks was not strong compared to the bright peak at 1.49 it is likely that it was there, but not captured.

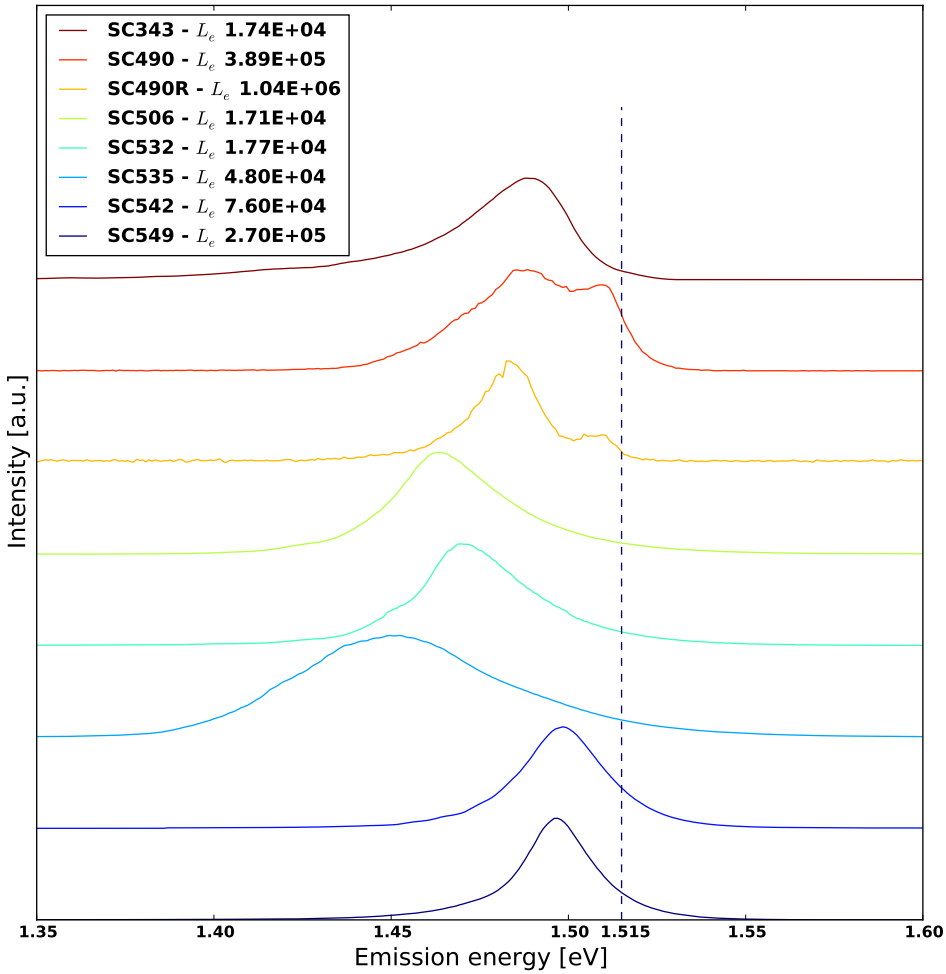

Figure 20: A representative measurement for each sample measured is shown at a power density of 565 W/cm^2. The vertical dashed line is where the 1.515 eV free exciton peak can be found if it is present. The intensity per second is shown as normalized to the highest intensity per second for each separate graph. The integrated intensity per second is also presented in the legend for each graph. Measurements were done at 12K.

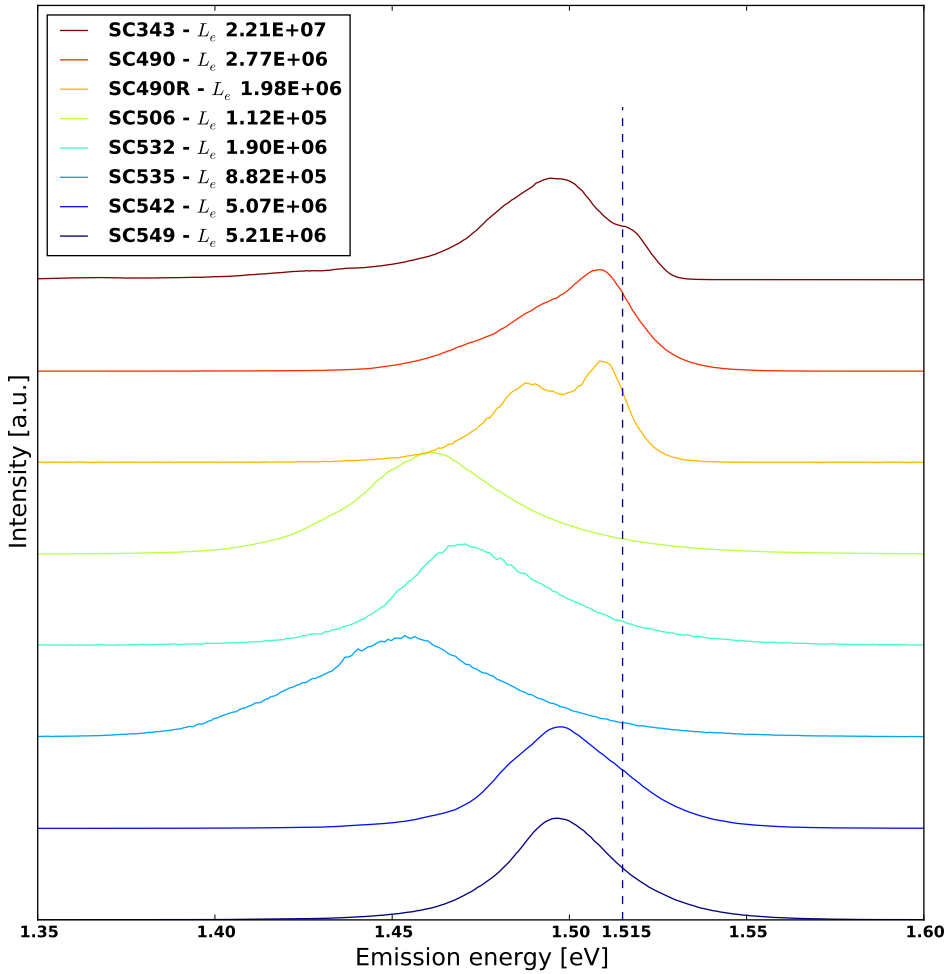

Figure 21: A representative measurement for each sample measured is shown at a power density of 5.7 kW/cm^2. The vertical dashed line is where the 1.515 eV free exciton peak can be found if it is present. The intensity per second is shown as normalized to the highest intensity per second for each separate graph. The integrated intensity per second is also presented in the legend for each graph. Measurements were done at 12K.

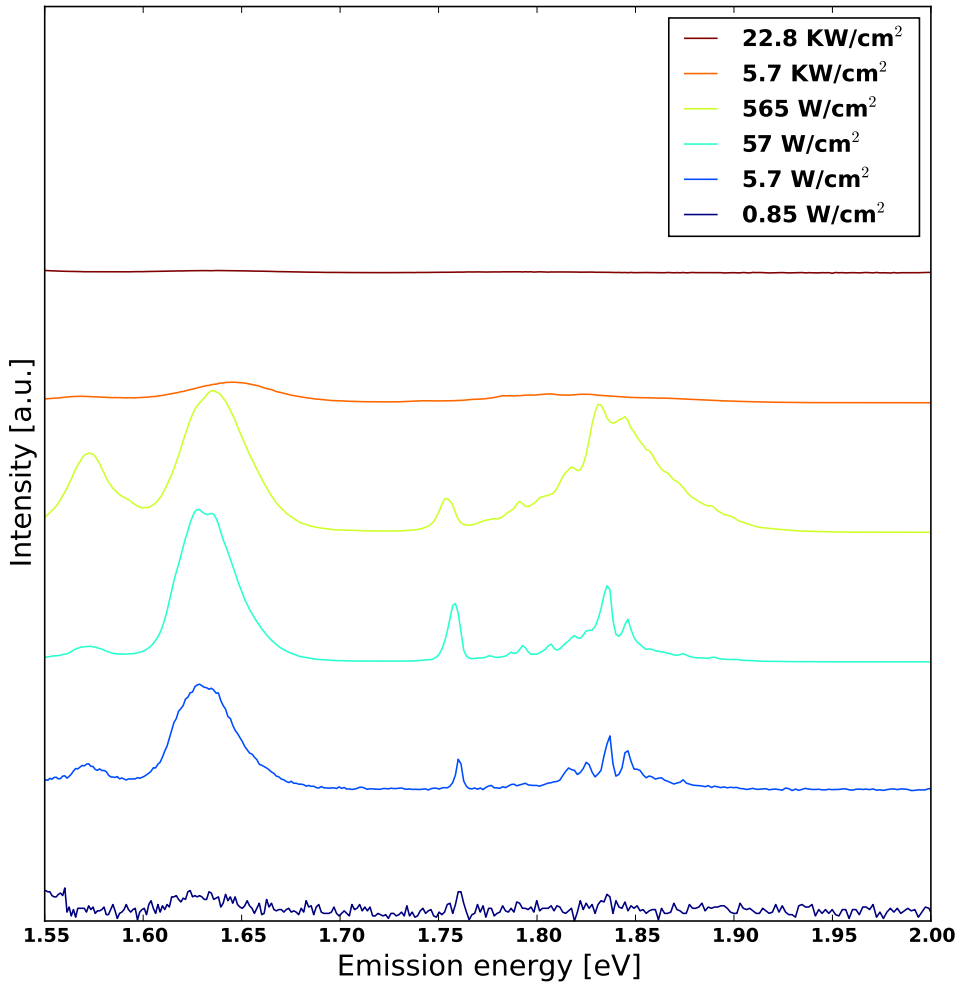

Figure 22: High intensity peaks observed from SC542, this can only be seen for this sample. However, previous growths using the same setup with similar parameters have also observed these peaks. This graphs in this plot is normalized to the highest value in the whole range, even what is outside of this observed window. This is done because the highest power density did not show any noticable emission in this region, while the second highest power density at 5.7kW/cm^2 shows some exication in this region, it is lower than what was measured for 565 W/cm^2. Measurements were done at 12K.

4.3.2 Single nanowire measurements

From the as grown results, the variation when doing PL measurements is small compared to the variation seen when analyzing the single nanowires. Because of this, more measurements are done. In figure 23 and 24 representative results from both the unpatterned and the patterned sample are presented. Thorugh all of the measurements done in this study, from only the random growth on SC490R can the free exciton peak be observed. The peaks at 565 W/cm^2 are consistent as seen from the error bars. The error bars represent the standard deviation of the peak location from measurements on 20 different NWs, this is true from SC490 as well.

What is surprising is that SC490 shows a peak at 1.51 eV when measured as grown, however for single nanowires this is not the case. No peaks could be observed above 1.48 eV in any of the measured NWs for this sample.

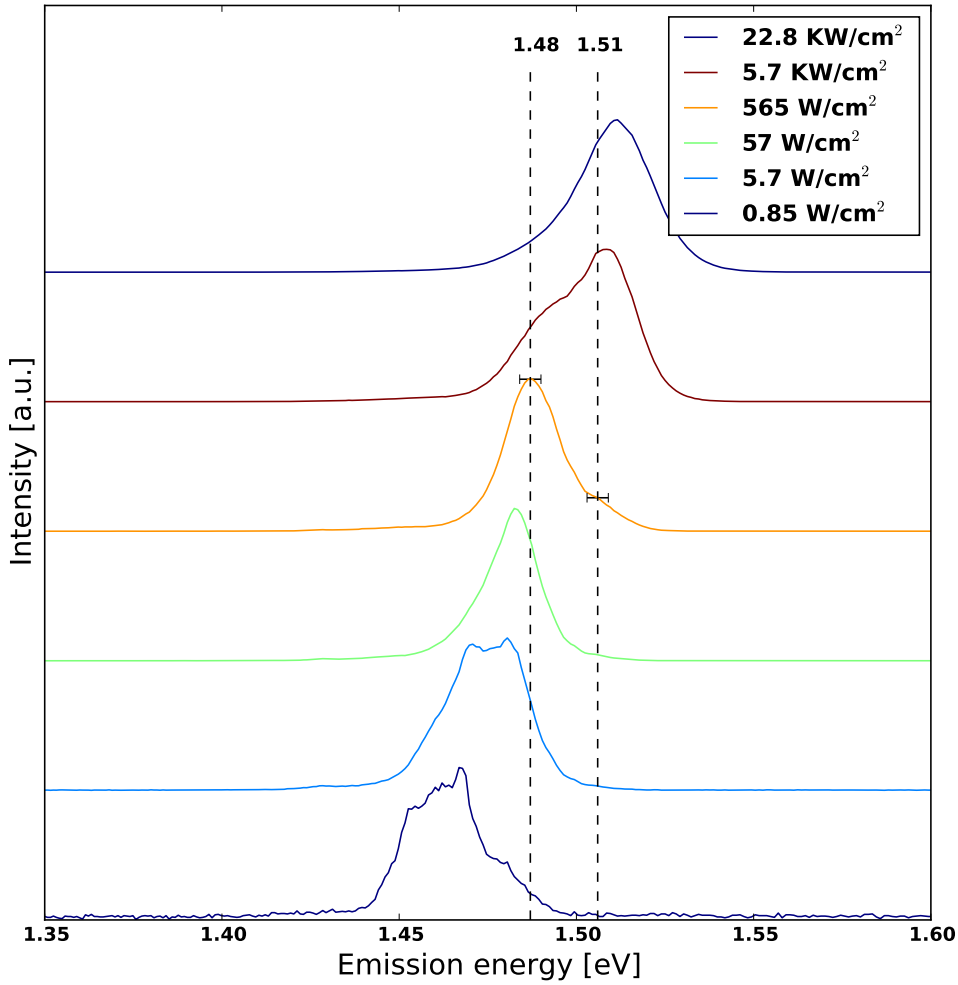

Figure 23: A representative NW from SC490R, this figure shows the peaks found when measuring the random growth sample. The intensity [a.u.] is plotted against the emission energy [eV]. The dashed lines indicate two peaks that recur for the 20 NWs measured from this sample. The error bars show the standard deviation of the peak position with a power density of 565 W/cm^2, i.e. the error bars are only valid for this power density. Measurements were done at 12K.

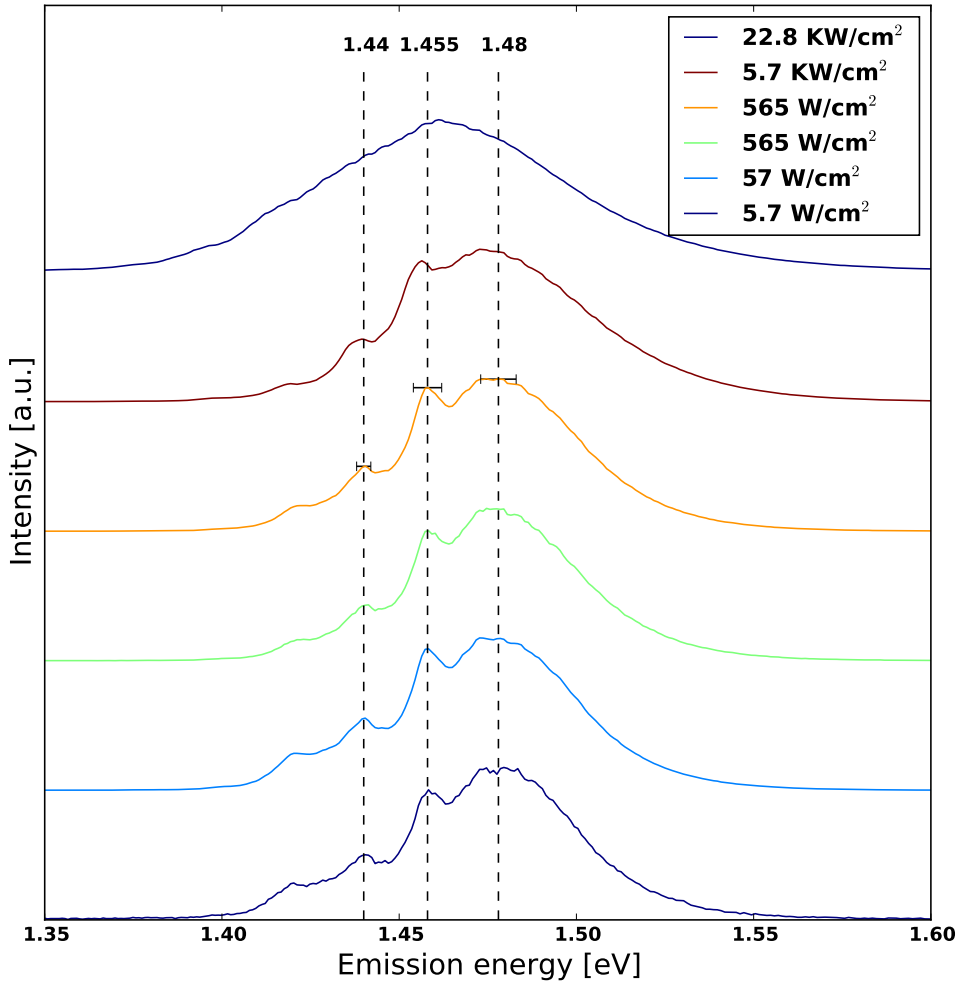

Figure 24: A representative NW from SC490, this figure shows the peaks found when measuring the random patterned sample. The dashed lines indicate three peaks that recur for the 20 NWs measured from this sample. The error bars show the standard deviation of the peak position with a power density of 565 W/cm^2, i.e. the error bars are only valid for this power density. Measurements were done at 12K.

5 Discussion

5.1 Growth

The aim of this study was to optimize growth conditions to achieve a good yield and get a good PL spectrum when measuring the grown sample. There were three main parameters that were changed in an effort to accomplish this; the As flux, the shell growth temperature, and whether there should be an axial insert or not. Prior to this study the growth had been optimized to give a good yield with uniform long (5+ μm) nanowires. SC490 was grown under these conditions as a starting point. From table 2 it is clear that the patterned growth of SC490 satisfied the previous criteria. The yield at 75.5 % is high, additionally the NWs were long at 5.6 μm and there was only a slight hourglass shape with the base and top of the nanowires almost identical in thickness. From a growth perspective this is a successful sample because of these criteria. SC490R which is the unpatterned sample grown at the same time as SC490 shows completely different characteristics, as it should. Because of the random growth conditions, nucleation could occur at any point on the wafer and thin-film growth is inevitable. If the goal had been to optimize growth conditions for unpatterned sample the uniformity could have been increased drastically with more standing NWs. This has been done previously. However, for the random growth, the goal was to try to understand where the energy peaks in PL measurements come from. The length and thickness is on average thinner than the patterned samples and highly variable. The reason for this is the parasitic 2D thin-film growth. This takes a away a lot of material that could otherwise have gone to the nanowires. Since the thin-film grows in grains, as seen in figure 16b, these will grow at an uneven pace depending on the angles of its facets and the structure around them. There is little merit to comparing the physical properties of SC490R to the rest, however, it is still useful for the PL discussion.

After measuring SC490 with the PL setup new samples were grown. The first change introduced was to increase the As flux. Since the As flux is the controlling element in regards to growth rate, this means that it is a faster grown nanowire than SC490. SC506 was grown with a higher As flux, with all other growth parameters kept to the same values except for the patterning process. The choice of patterning process was not done intentionally, but based on availability. This adds another parameter of uncertainty. Because of this uncertainty it is hard to draw conclusions as to why the yield reduced to 37.4 % as observed for SC506, however, the pattern is a likely candidate. Looking at the physical characteristics from these nanowires, the thickness sticks out. Both at the base and top, SC506 is over 50 % thicker than SC490. This can be attributed to the pattern, since no other samples come close to this thickness and SC506 was the only sample grown on a new type of NIL pattern. These patterns proved to be faulty in that the hole size was larger than intended, which further helps explain the thickness discrepancy. The larger holes can also help explain the yield. Since larger holes changes how the droplets nucleate. In figure 17b the SEM image from SC506 shows that it has large grains where nanowires are missing. A possible explanation is that two or more droplets nucleate in the same hole which leads them to grow into each other.

SC532 which was the attempt at regrowing SC343 was grown on the same NIL substrate as used to grow SC343. Furthermore, this sample was grown with both a higher shell temperature and an axial insert. With a total of three parameters changed in comparison to

SC490 it is difficult to state specific reasons for the observed physical properties or why they differ.

SC535 is the only anti-tapered NW growth in this study. These are also the only NWs grown with a As flux lower than 3.1E-6. Compared to SC490 only one parameter has been intentionally changed. However, as mentioned earlier in chapter 4.1 the oxidation buildup is also a factor. To combat the oxidation a longer HF etch was performed before growth commenced. The yield is lower than for SC490, however, at 56.3 % the yield is acceptable. It is highly likely that the anti-tapering stems from the low As flux. In the SEM image in figure 17d the anti-tapering, as well as the solidified droplet, can be seen for some NWs. This sample had a very long growth time compared to other samples. This is due to the low As flux which means a slower deposition. The NWs on SC535 are shorter than SC490, this is likely due to the anti-tapering. Since there is a larger droplet, i.e. larger area, it is necessary with more material to grow each new monolayer.

SC549 is identical to SC542, with the exception that the SC549 had been less exposed to oxidation. The yield show how much of an effect native oxidation can have. The NW length is the same for the two samples, while the thickness is different. However, the ratio between the thickness at the base and the thickness at the top is 1 % different for the two samples relative to SC549. Hole width is the reason the thickness is different between the two samples, and this also impacts the yield. The SEM image of SC542 in figure 17e shows similar grains in the holes as SC506 does. Compared to SC490 there is a higher As flux as well as a higher shell growth temperature for SC542 and SC549. SC549 does not show the same quality in terms of height and yield as SC549, there are also some visible droplets in SC549. However, considering SC490 had minimal waiting time between patterning and growth, the result for SC549 could have been even better if it had been less exposed to oxidation.

5.2 Intensity

When discussing the intensity observed in the samples it is important to note that this is the result that is most prone to errors. Not only have there been done various steps of calibration, but where the focus of the beam is places also matters greatly. That being said, there are some results that can be used to discuss the intensity.

As mentioned in chapter 4.2 the as grown measurements show a higher integrated intensity per second than single nanowire measurements. However, both of these measurements the results follow the same trends. From the random growth SC490R a higher intensity can be observed at low power densities compared to the rest of the measurements. This is despite the fact that the average dimensions for the random growth is smaller than all other samples. Therefore, when exciting SC490R single nanowires there is less surface area where excitation can occur. This might be a reason why, for higher power densities, the other samples have a stronger intensity. Both SC 490R and SC490 emits stronger than most other by at least one order of magnitude for low power densities in the as grown measurements. For single NWs, although there are more measurements done, there is too much variation to say if this is the case here as well. What can be gathered from figure 19 is that nanowires from the different growths showed on average a similar trend. Among these measurements there were deviants, with either a very high or a very low integrated intensity per second, but this cannot give any further information.

The emitted intensity from SC343 is on par with the samples analyzed in this study. While SC506 shows a strange behavior for the two highest power densities in the as grown measurements. However, when looking at the single NW measurements there does not seem to be any discrepancy between SC506 and SC490. That makes it plausible that it was an error in the measurement, even though the as grown sample was measured at various positions.

It is not possible to say anything about the effect of the shell growth temperature, or the axial insert that some samples have based on the integrated intensity per second other than that it does not appear to affect the emitted intensity noticeably.

5.3 Energy levels

Optimizing parameters for growth such that a free exciton emission could be found was the goal of this study. SC343, shows this behaviour with a peak around 1.515 as seen in figure 21. Additionally, SC343 has a decent yield at 59.3 % and with a length of 5.7 μm have long NWs. From an eariler master thesis, measuring SC343 as both as grown and single NWs [29] a free exciton emission was found for both. SC490 and SC490R showed promising results when measured as grown. Both SC490R and SC490 has an energy peak around 1.51 eV, which coincides well with the free exciton emission. However, when measured as single nanowires only SC490R showed a peak around 1.51. SC490 did not show any measureable emission above 1.48 eV. Despite SC490R having a good PL spectrum, it is a random growth sample. To create a device from NWs it is generally preffered, or even necessary to have a patterned growth. Furthermore, the large variation in sizes from the random growth makes them undesirable. This is why a good PL spectrum for patterned growth was pursued.

It is difficult to pin down the reason why the free exciton emission present in the as grown measurements were not found in single NW measurements for SC490. Some possible explanations are that the NWs not present, i.e. where the there is not grow a NW in the hole, somehow contributed to this free exciton emission. This is however unlikely since other growths with lower yield, and therefore more missing NWs does not show this behavior. A second explanation that was throughly investigated was the chance that the sample was not cooled properly. That the thermal contact between the TEM grid and cold finger in the cryostat was poor. However, to rule out this possibility, the measurements were repeated several times at different occasions with a complete shutdown, and repositioning of the TEM grid. Additionally, NWs from SC490 was distributed on a Si substrate to ensure that the problem was not the cooling of the sample. All these additional measurements corroborated what is seen in figure 24, it is highly unlikely that this is indeed the reason for why there are no observed emission at 1.51 eV. A third and more likely reason is that the emission observed in the as grown sample stems from a part of the NW that is not dominating when measuring single NWs. As grown samples are measured from the top down with the focus of the laser light somewhere along the nanowire. This means that the highest power density can be at various heights for the as grown measurements. Where on the nanowire the focus is cannot be controlled intentionally. Instead, if there is any observed intensity at 1.51 the focus is done such that this peak is maximized. If there is no peak around 1.51 the closest peak in terms of emission energy is maximized. Single NWs are measured while laying down. Investigations were done to see if the laser could

be focused on the base or the top of the NW. However, due to the spot size of the laser, it did not make a meaningful difference on where on the nanowire the laser focus was aimed. Furthermore, even if this could be done, it is in many cases not possible to say which end is the top or the base because the wires are broken off. The three peaks observed for single NWs in SC490 were consistent. In all the mesured NWs these were present when the power density was 565 W/cm^2. This means that these peaks are not random, and most likely stem from stacking faults and type-II transitions.

For the other samples there was a great spread of where the strongest peak ended up in terms of emission energy. It is very hard to draw any hard conclusion when looking at figures 20 and 21, and comparing this to the key differences in growth parameters in table 1. As stated in chapter 4.3.1, SC535 which was grown with a much lower As flux, and therefore slower growth rate, sticks out. This sample has a broad energy peak centered around 1.45 eV. It is likely that the slow growth rate created stacking faults which is responsible for this low emission energy.

SC542 emitted at high energies for one of the measurements. This has also been observed in previous samples. Although only one measurement showed this result, something that was done every time a new sample was measured was to scan across the surface of the sample with the beam. While scanning across the real time results were observed, and the focus adjusted randomly. This behavior was observed at several locations, however, it was not dominant for the majority of the sample. From previous samples it was assumed that this occurs when growing the AlGaAs shell at high temperatures. This results supports that claim, however, since it was not found for any other samples it is again difficult to be certain.

SC542 and SC549 were grown with the same parameters, which is reflected in figure 20 and 21. It is interesting to see that despite SC 542 being thicker and having a lower yield, resulting in more 2D growth, it does not change the energy of the emitted signal.

Room temperature measurements were also performed, however, because the peaks at low temperatures did not show any free exciton emission, these results does not give any additional information. They have therefore not been inlcuded

5.4 Uncertainties

There is a large variety of errors during these measurements. The first starting with the fact that the samples were grown on different patterned substrates, as well as time affecting the oxide layer. This makes it very hard to optimize growth. If samples truly are to be grown under the same conditions, there needs to be a batch growth, one after another with one parameter varied at a time. Growing and then analyzing the results from the SEM images, and PL spectra means there is too much time between each growth and the conditions will have changed.

Another error source is the optical setup, which is highly sensitive to disturbances. To be able to measure accurately for each sample it is necessary to optimize the setup. This is done by adjusting mirrors. For each new temperature the focus of the beam needs adjustment. In this process interpretation is needed. It is possible to focus the beam on the silicon substrate and have resulting emission peaks at some place where they are not expected for GaAs. In the same manner, the focus can be at different parts of the NWs. The purpose of these measurements were to optimize the growth for free exciton

emission. Therefore, for each new temperature measurement, the closest emission to 1.51 eV in terms of energy was maximized for intensity at this peak. The focusing can therefore end up being done in a different manner for different locations/NWs.

6 Conclusion and future outlook

Six different growth conditions have been analyzed in an effort to grow nanowires emitting at an energy level close to the free exciton emission. This has not been achieved, and due to a great variation in parameters between each sample it is hard to draw any conclusion. E.g. the integrated intensity is not able to give much additional information because of the variety of parameters changed between each sample. However, despite different sizes of the NWs and different yield, SC542 and SC549 have a almost identical PL emission. This is interesting to note for future growths. Furthermore, decreasing the As flux too much, gives anti-tapered nanowires with a low emission peak. Energy peaks in all ranges from 1.45 eV to 1.51 eV have been observed for as grown measurements. However, the only patterned sample that showed the peaks at 1.51 eV did not have these peaks when measured as individual nanowires. There seems to be no clear connection between the axial insert and the energy levels observed, nor to the integrated intensity observed. The same is true for the high temperature AlGaAs shell growth. This does not seem to have any clear effect on the PL spectrum, other than potentially yielding high energy peaks at 1.85 eV.

Further growths should be done in stricter conditions, i.e. more identical conditions, limiting parameters changed as well as reducing uncertainties.

For the future, doing a batch growth varying only one parameter at the time may give additional insight into what affects the emitted energy levels as well as the yield. Additionally, doing TEM on these samples could give information on where stacking faults are located, which could make it possible to avoid these faults. A third investigation that would yield valuable information is cathodoluminescence (CL), this would give information on where in each nanowire the different emission energies stem from. Using this in conjunction with TEM results, would allow for an analysis on how stacking faults affect the emitted signal. CL would also give information on which parts of the nanowire emits strongest.

References

[1] A. R. Gobat, M. F. Lamorte, and G. W. McIver. Characteristics of High-Conversion-Efficiency Gallium-Arsenide Solar Cells. *IRE Transactions on Military Electronics*, MIL-6(1):20–27, January 1962.

[2] JS Blakemore. Semiconducting and other major properties of gallium arsenide. *Journal of Applied Physics*, 53:R123–R181, 1982.

[3] S.-S. Beyertt, U. Brauch, F. Demaria, N. Dhidah, a. Giesen, T. Kubler, S. Lorch, F. Rinaldi, and P. Unger. Efficient Gallium–Arsenide Disk Laser. *IEEE Journal of Quantum Electronics*, 43(10):869–875, October 2007.

[4] Rüdeger Köhler, Alessandro Tredicucci, Fabio Beltram, Harvey E Beere, Edmund H Linfield, A Giles Davies, David A Ritchie, Rita C Iotti, and Fausto Rossi. Terahertz semiconductor-heterostructure laser. *Nature*, 417(6885):156–9, May 2002.

[5] Martin A. Green, Keith Emery, Yoshihiro Hishikawa, Wilhelm Warta, and Ewan D. Dunlop. Solar cell efficiency tables (version 39). *Progress in Photovoltaics: Research and Applications*, 20(1):12–20, January 2012.

[6] Peidong Yang, Ruoxue Yan, and Melissa Fardy. Semiconductor nanowire: what's next? *Nano letters*, 10(5):1529–36, May 2010.

[7] Fang Qian and Charles M. Lieber. Semiconductor Nanowire Lasers. In *LEOS 2007 - IEEE Lasers and Electro-Optics Society Annual Meeting Conference Proceedings*, pages 831–831. IEEE, October 2007.

[8] Wei Lu, Ping Xie, and Charles M. Lieber. Nanowire Transistor Performance Limits and Applications. *IEEE Transactions on Electron Devices*, 55(11):2859–2876, November 2008.

[9] L. Tsakalakos, J. Balch, J. Fronheiser, B. A. Korevaar, O. Sulima, and J. Rand. Silicon nanowire solar cells. *Applied Physics Letters*, 91(23):233117, 2007.

[10] Steffen Breuer, Carsten Pfüller, Timur Flissikowski, Oliver Brandt, Holger T Grahn, Lutz Geelhaar, and Henning Riechert. Suitability of Au- and self-assisted GaAs nanowires for optoelectronic applications. *Nano letters*, 11(3):1276–9, March 2011.

[11] Toshihide Takagahara and Kyozaburo Takeda. Theory of the quantum confinement effect on excitons in quantum dots of indirect-gap materials. *Physical Review B*, 46(23):15578–15581, December 1992.

[12] Ruoxue Yan, Daniel Gargas, and Peidong Yang. Nanowire photonics. *Nature Photonics*, 3(10):569–576, October 2009.

[13] G.H. Olsen. Interfacial lattice mismatch effects in III–V compounds. *Journal of Crystal Growth*, 31:223–239, December 1975.

[14] Karen L Kavanagh. Misfit dislocations in nanowire heterostructures. *Semiconductor Science and Technology*, 25(2):024006, February 2010.

[15] R. S. Wagner and W. C. Ellis. Vapor-liquid-solid mechanism of single crystal growth. *Applied Physics Letters*, 4(5):89, 1964.

[16] R. L. Barns and W. C. Ellis. Whisker Crystals of Gallium Arsenide and Gallium Phosphide Grown by the Vapor—Liquid—Solid Mechanism. *Journal of Applied Physics*, 36(7):2296, July 1965.

[17] Xiangfeng Duan, Jianfang Wang, and Charles M. Lieber. Synthesis and optical properties of gallium arsenide nanowires. *Applied Physics Letters*, 76(9):1116, February 2000.

[18] Soo-Ghang Ihn, Jong-In Song, Tae-Wook Kim, Dong-Seok Leem, Takhee Lee, Sang-Geul Lee, Eui Kwan Koh, and Kyung Song. Morphology- and orientation-controlled gallium arsenide nanowires on silicon substrates. *Nano letters*, 7(1):39–44, January 2007.

[19] W. R. Wilcox and T. J. LaChapelle. Mechanism of Gold Diffusion into Silicon. *Journal of Applied Physics*, 35(1):240, July 1964.

[20] Maya Bar-Sadan, Juri Barthel, Hadas Shtrikman, and Lothar Houben. Direct imaging of single Au atoms within GaAs nanowires. *Nano letters*, 12(5):2352–6, May 2012.

[21] A. Fontcuberta i Morral, C. Colombo, G. Abstreiter, J. Arbiol, and J. R. Morante. Nucleation mechanism of gallium-assisted molecular beam epitaxy growth of gallium arsenide nanowires. *Applied Physics Letters*, 92(6):063112, February 2008.

[22] D. Spirkoska, J. Arbiol, A. Gustafsson, S. Conesa-Boj, F. Glas, I. Zardo, M. Heigoldt, M. H. Gass, A. L. Bleloch, S. Estrade, M. Kaniber, J. Rossler, F. Peiro, J. R. Morante, G. Abstreiter, L. Samuelson, and A. Fontcuberta I Morral. Structural and optical properties of high quality zinc-blende/wurtzite GaAs nanowire heterostructures. *Physical Review B - Condensed Matter and Materials Physics*, 80(24):245325, December 2009.

[23] G. E. Cirlin, V. G. Dubrovskii, Yu. B. Samsonenko, A. D. Bouravleuv, K. Durose, Y. Y. Proskuryakov, Budhikar Mendes, L. Bowen, M. A. Kaliteevski, R. A. Abram, and Dagou Zeze. Self-catalyzed, pure zincblende GaAs nanowires grown on Si(111) by molecular beam epitaxy. *Physical Review B*, 82(3):035302, July 2010.

[24] WS Knodle and Robert Chow. Molecular Beam Epitaxy Equipment and Practice. *Thin-Film Deposition Processes and Technologies*, pages 381–461, 2002.

[25] Sadao Adachi. *Properties of Aluminium Gallium Arsenide*. IET, no. 7 edition, 1993.

[26] Benedikt Mayer, Daniel Rudolph, Joscha Schnell, Stefanie Morkötter, Julia Winnerl, Julian Treu, Kai Müller, Gregor Bracher, Gerhard Abstreiter, Gregor Koblmüller, and Jonathan J Finley. Lasing from individual GaAs-AlGaAs core-shell nanowires up to room temperature. *Nature communications*, 4:2931, January 2013.

[27] A M Munshi, D L Dheeraj, V T Fauske, D C Kim, J Huh, J F Reinertsen, L Ahtapodov, K D Lee, B Heidari, a T J van Helvoort, B O Fimland, and H Weman. Position-controlled uniform GaAs nanowires on silicon using nanoimprint lithography. *Nano letters*, 14(2):960–6, February 2014.

[28] Abdul Mazid Munshi. *Epitaxial Growth of Self-Catalyzed GaAs Nanowires by Molecular Beam Epitaxy*. Doctoral thesis, Norwegian University of Science and Technology, 2014.

[29] Stian Gulla. *Advanced Micro Photoluminescence Spectroscopy of Single GaAs/AlGaAs Core-Shell Nanowires*. Master thesis, Norwegian University of Science and Technology, 2013.

[30] L. Ahtapodov, A. M. Munshi, J. S. Nilsen, J. F. Reinertsen, D. L. Dheeraj, B. O. Fimland, A. T. J. van Helvoort and H. Weman. Effect of III/V-ratio on the structural and optical Properties of Self-Catalyzed GaAs Nanowires. page 24.

[31] A De and CE Pryor. Predicted band structures of III-V semiconductors in the wurtzite phase. *Physical Review B*, 52242, 2010.

[32] Charles Kittel. *Introduction to solid state physics*. Wiley, 8th edition, 2005.

[33] Michael Quirk & Julian Serda. *Semiconductor Manufacturing Technology*. Pearson, 1st edition, 2001.

[34] Thomas Må rtensson, C. Patrik T. Svensson, Brent A. Wacaser, Magnus W. Larsson, Werner Seifert, Knut Deppert, Anders Gustafsson, L. Reine Wallenberg, and Lars Samuelson. Epitaxial III-V Nanowires on Silicon. *Nano Letters*, 4(10):1987–1990, October 2004.

[35] N. Wang, Y. Cai, and R.Q. Zhang. Growth of nanowires. *Materials Science and Engineering: R: Reports*, 60(1-6):1–51, March 2008.

[36] Peter Krogstrup, Ronit Popovitz-Biro, Erik Johnson, Morten Hannibal Madsen, Jesper Nygå rd, and Hadas Shtrikman. Structural phase control in self-catalyzed growth of GaAs nanowires on silicon (111). *Nano letters*, 10(11):4475–82, November 2010.

[37] Martin C. Peckerar Harry J. Levinson, Mark A. McCord, Franco Cerrina, Robert D. Allen, John G. Skinner, Andrew R. Neureuther. Handbook of Microlithography, Micromachining, and Microfabrication. Volume 1: Microlithography (SPIE Press Monograph Vol. PM39), 1997.

[38] S. Y. Chou, P. R. Krauss, and P. J. Renstrom. Imprint Lithography with 25-Nanometer Resolution. *Science*, 272(5258):85–87, April 1996.

[39] John R. Arthur. Molecular beam epitaxy. *Surface Science*, 500(1-3):189–217, March 2002.

[40] N. Inoue. MBE monolayer growth control by in-situ electron microscopy. *Journal of Crystal Growth*, 111(1-4):75–82, May 1991.

[41] Ayahiko Ichimiya and Philip I. Cohen. *Reflection High-Energy Electron Diffraction*. Cambridge University Press, 2004.

[42] Alfred B. Anderson. Derivation of the extended Hückel method with corrections: One electron molecular orbital theory for energy level and structure determinations. *The Journal of Chemical Physics*, 62(3):1187, September 1975.

[43] John Clarke Slater. *Quantum theory of molecules and solids*, volume v.1. McGraw-Hill, New York, NY, v.1 edition, 1963.

[44] John Clarke Slater. Damped Electron Waves in Crystals. *Physical Review*, 51(10):840–846, May 1937.

[45] Wikimedia. Band filling diagram, June 2013. `http://commons.wikimedia.org/wiki/File:Band_filling_diagram.svg` accessed 03.09.2014.

[46] Mark Hybertsen and Steven Louie. Electron correlation in semiconductors and insulators: Band gaps and quasiparticle energies. *Physical Review B*, 34(8):5390–5413, October 1986.

[47] C. Hwang. Densities of states and properties of spontaneous and stimulated emission in semiconductor lasers. *IEEE Journal of Quantum Electronics*, 6(6):310–310, June 1970.

[48] Herbert S. Bennett. High dopant and carrier concentration effects in gallium aluminum arsenide: Densities of states and effective intrinsic carrier concentrations. *Journal of Applied Physics*, 83(6):3102, 1998.

[49] Thomas Elsaesser, Jagdeep Shah, Lucio Rota, and Paolo Lugli. Initial thermalization of photoexcited carriers in GaAs studied by femtosecond luminescence spectroscopy. *Physical Review Letters*, 66(13):1757–1760, April 1991.

[50] Sadao Adachi. *GaAs and related materials*. World Scientific, 1994.

[51] V. Gurevich and A. Thellung. Quasimomentum in the theory of elasticity and its conservation. *Physical Review B*, 42(12):7345–7349, October 1990.

[52] James Chelikowsky and Marvin Cohen. Nonlocal pseudopotential calculations for the electronic structure of eleven diamond and zinc-blende semiconductors. *Physical Review B*, 14(2):556–582, July 1976.

[53] Marvin Cohen and T. Bergstresser. Band Structures and Pseudopotential Form Factors for Fourteen Semiconductors of the Diamond and Zinc-blende Structures. *Physical Review*, 141(2):789–796, January 1966.

[54] S Richard, F Aniel, and G Fishman. Energy-band structure of Ge, Si, and GaAs: A thirty-band k center dot p method. *Physical Review B*, 70:–, 2004.

[55] Chia-Chi Chang, Chun-Yung Chi, Maoqing Yao, Ningfeng Huang, Chun-Chung Chen, Jesse Theiss, Adam W Bushmaker, Stephen Lalumondiere, Ting-Wei Yeh, Michelle L Povinelli, Chongwu Zhou, P Daniel Dapkus, and Stephen B Cronin. Electrical and optical characterization of surface passivation in GaAs nanowires. *Nano letters*, 12(9):4484–9, September 2012.

[56] D.J. Fitzgerald and A.S. Grove. Surface recombination in semiconductors. In *1967 International Electron Devices Meeting*, volume 13, pages 102–104. IRE, 1967.

[57] D. Stukel and R. Euwema. Energy-Band Structure of Aluminum Arsenide. *Physical Review*, 188(3):1193–1196, December 1969.

[58] Sadao Adachi. GaAs, AlAs, and Al[sub x]Ga[sub 1 - x]As@B: Material parameters for use in research and device applications. *Journal of Applied Physics*, 58:R1–R29, 1985.

[59] W. Spitzer and H. Fan. Determination of Optical Constants and Carrier Effective Mass of Semiconductors. *Physical Review*, 106(5):882–890, June 1957.

[60] W Y Liang. Excitons. *Physics Education*, 5(4):226–228, July 1970.

[61] Gregory Wannier. The Structure of Electronic Excitation Levels in Insulating Crystals. *Physical Review*, 52(3):191–197, August 1937.

[62] N. F. Mott. Metal-Insulator Transition. *Reviews of Modern Physics*, 40(4):677–683, October 1968.

[63] S. Perera, M. A. Fickenscher, H. E. Jackson, L. M. Smith, J. M. Yarrison-Rice, H. J. Joyce, Q. Gao, H. H. Tan, C. Jagadish, X. Zhang, and J. Zou. Nearly intrinsic exciton lifetimes in single twin-free GaAs/AlGaAs core-shell nanowire heterostructures. *Applied Physics Letters*, 93(5):053110, August 2008.

[64] G. Vektaris. A new approach to the molecular biexciton theory. *The Journal of Chemical Physics*, 101(4):3031, August 1994.

[65] Thang B. Hoang, A. F. Moses, H. L. Zhou, D. L. Dheeraj, B. O. Fimland, and H. Weman. Observation of free exciton photoluminescence emission from single wurtzite GaAs nanowires. *Applied Physics Letters*, 94(13):133105, April 2009.

[66] Neimantas Vainorius, Daniel Jacobsson, Sebastian Lehmann, Anders Gustafsson, Kimberly a. Dick, Lars Samuelson, and Mats-Erik Pistol. Observation of type-II recombination in single wurtzite/zinc-blende GaAs heterojunction nanowires. *Physical Review B*, 89(16):165423, April 2014.

[67] U. Jahn, J. Lähnemann, C. Pfüller, O. Brandt, S. Breuer, B. Jenichen, M. Ramsteiner, L. Geelhaar, and H. Riechert. Luminescence of GaAs nanowires consisting of wurtzite and zinc-blende segments. *Physical Review B - Condensed Matter and Materials Physics*, 85(4), 2012.

[68] F. Möglich and R. Rompe. Über den Einflußder Wärmedehnung auf das Absorptionsspektrum von Isolatoren. *Zeitschrift für Physik*, 119(7-8):472–481, 1942.

[69] Y.P. Varshni. Temperature dependence of the energy gap in semiconductors. *Physica*, 34(1):149–154, 1967.

[70] P. Debye. Zur Theorie der spezifischen Wärmen. *Annalen der Physik*, 344(14):789–839, 1912.

[71] K. P. O'Donnell and X. Chen. Temperature dependence of semiconductor band gaps. *Applied Physics Letters*, 58(25):2924, June 1991.

[72] E. Bogardus and H. Bebb. Bound-Exciton, Free-Exciton, Band-Acceptor, Donor-Acceptor, and Auger Recombination in GaAs. *Physical Review*, 176(3):993–1002, December 1968.

[73] H.-R. Höche and J. Schreiber. Anisotropic deformation behaviour of GaAs. *Physica Status Solidi (a)*, 86(1):229–236, November 1984.

[74] Jing Liqiang, Qu Yichun, Wang Baiqi, Li Shudan, Jiang Baojiang, Yang Libin, Fu Wei, Fu Honggang, and Sun Jiazhong. Review of photoluminescence performance of nano-sized semiconductor materials and its relationships with photocatalytic activity. *Solar Energy Materials and Solar Cells*, 90(12):1773–1787, July 2006.

[75] Martin Feneberg, Sarah Osterburg, Karsten Lange, Christian Lidig, Bernd Garke, Rüdiger Goldhahn, Eberhard Richter, Carsten Netzel, Maciej D. Neumann, Norbert Esser, Stephanie Fritze, Hartmut Witte, Jürgen Bläsing, Armin Dadgar, and Alois Krost. Band gap renormalization and Burstein-Moss effect in silicon- and germanium-doped wurtzite GaN up to 10ˆ20. *Physical Review B*, 90(7):075203, August 2014.

[76] L. Jay Guo. Nanoimprint lithography: Methods and material requirements. *Advanced Materials*, 19(4):495–513, February 2007.